JAMES | Journal of Advances in Modeling Earth Systems®

RESEARCH ARTICLE
10.1029/2024MS004599

Incorporating the Acclimation of Photosynthesis and Leaf Respiration in the Noah-MP Land Surface Model: Model Development and Evaluation

Yanghang Ren[1], Han Wang[1], Sandy P. Harrison[1,2], I. Colin Prentice[1,3], Giulia Mengoli[3], Long Zhao[4], Peter B. Reich[5,6,7], and Kun Yang[1]

[1]Department of Earth System Science, Ministry of Education Key Laboratory for Earth System Modeling, Institute for Global Change Studies, Tsinghua University, Beijing, China, [2]School of Archaeology, Geography and Environmental Sciences (SAGES), University of Reading, Reading, UK, [3]Department of Life Sciences, Georgina Mace Centre for the Living Planet, Imperial College London, Silwood Park Campus, Ascot, UK, [4]Chongqing Jinfo Mountain Karst Ecosystem National Observation and Research Station, School of Geographical Sciences, Southwest University, Chongqing, China, [5]Department of Forest Resources, University of Minnesota, St. Paul, MN, USA, [6]Institute for Global Change Biology, and School for the Environment and Sustainability, University of Michigan, Ann Arbor, MI, USA, [7]Hawkesbury Institute for the Environment, Western Sydney University, Penrith, NSW, Australia

Key Points:

- The new scheme captures the observed temporal and spatial variations in $V_{cmax,25}$ and R_{25} that are not considered in the standard scheme
- The new scheme improves photosynthesis and leaf respiration predictions across biomes
- The new representations of photosynthesis and leaf respiration result in greater net CO_2 uptake by land ecosystems

Supporting Information:

Supporting Information may be found in the online version of this article.

Correspondence to:

H. Wang,
wang_han@mail.tsinghua.edu.cn

Citation:

Ren, Y., Wang, H., Harrison, S. P., Prentice, I. C., Mengoli, G., Zhao, L., et al. (2025). Incorporating the acclimation of photosynthesis and leaf respiration in the Noah-MP land surface model: Model development and evaluation. *Journal of Advances in Modeling Earth Systems*, *17*, e2024MS004599. https://doi.org/10.1029/2024MS004599

Received 25 JUL 2024
Accepted 10 FEB 2025

Abstract Realistic simulation of leaf photosynthetic and respiratory processes is needed for accurate prediction of the global carbon cycle. These two processes systematically acclimate to long-term environmental changes by adjusting photosynthetic and respiratory traits (e.g., the maximum photosynthetic capacity at 25°C ($V_{cmax,25}$) and the leaf respiration rate at 25°C (R_{25})) following increasingly well-understood principles. While some land surface models (LSMs) now account for thermal acclimation, they do so by assigning empirical parameterizations for individual plant functional types (PFTs). Here, we have implemented an Eco-Evolutionary Optimality (EEO)-based scheme to represent the universal acclimation of photosynthesis and leaf respiration to multiple environmental effects, and that therefore requires no PFT-specific parameterizations, in a standard version of the widely used LSM, Noah MP. We evaluated model performance with plant trait data from a 5-year experiment and extensive global field measurements, and carbon flux measurements from FLUXNET2015. We show that observed R_{25} and $V_{cmax,25}$ vary substantially both temporally and spatially within the same PFT (*C.V.* >20%). Our EEO-based scheme captures 62% of the temporal and 70% of the spatial variations in $V_{cmax,25}$ (73% and 54% of the variations in R_{25}). The standard scheme underestimates gross primary production by 10% versus 2% for the EEO-based scheme and generates a larger spread in r (correlation coefficient) across flux sites (0.79 ± 0.16 vs. 0.84 ± 0.1, mean ± S.D.). The standard scheme greatly overestimates canopy respiration (bias: ∼200% vs. 8% for the EEO scheme), resulting in less CO_2 uptake by terrestrial ecosystems. Our approach thus simulates climate-carbon coupling more realistically, with fewer parameters.

Plain Language Summary Understanding how leaves absorb and release carbon dioxide (CO_2) is important to predict the dynamics of CO_2 in the atmosphere. In the face of environmental changes, plants adjust their basal photosynthetic and respiratory characteristics (traits). Most land surface models assume these characteristics are constant for a given plant type, or use empirical relationships to characterize their variations. To address this issue, we incorporated a new scheme that accounts for the adjustments of these characteristics to various environmental factors in a land surface model and tested it with global plant trait data and carbon flux measurements. The new scheme captures most of the variation of photosynthetic and respiratory traits across different locations and over time. It also reliably predicts the amount of carbon absorbed and released by leaves at different time scales. Compared to observations, the standard model underestimates the amount of carbon absorbed by plants and overestimates the amount released. The new scheme has fewer parameters than the standard one and is simple to implement. Its incorporation in other land surface models should also provide realistic predictions of land CO_2 uptake in a changing world.

1. Introduction

The terrestrial biosphere acts as a carbon sink, currently removing approximately one-third of total anthropogenic emissions and thereby slowing the rate of climate change (Arneth et al., 2010; Arora & Montenegro, 2011;

Bonan, 2008; Piao et al., 2009). Carbon enters terrestrial ecosystems through photosynthesis, which is responsible for a global uptake of approximately 120–150 Pg C yr^{-1} (i.e., gross primary production, GPP) (Anav et al., 2015; Beer et al., 2010; Jiang & Ryu, 2016; Stocker et al., 2020). About half of the CO_2 emission by plants to the atmosphere is released by respiration from canopy leaves (R_{canopy}) (Atkin et al., 2014; Reich et al., 1998), and small fractional changes in R_{canopy} can thus have large impacts on ecosystem functioning (Piao et al., 2010). Leaf respiration breaks down photosynthetic products and provides energy to support the protein turnover required to maintain photosynthetic capacity (Reich et al., 2021; Ren et al., 2023; Wang et al., 2020). The residual between GPP and R_{canopy} determines the amount of carbon allocated to the ecosystem and dominates terrestrial ecosystem exchange, showing large year-to-year variability in response to environmental changes (Keenan & Williams, 2018; Wang et al., 2023). Accurate modeling of GPP and R_{canopy} is therefore important for reliable predictions of the magnitude of the potential land carbon sink (Bonan et al., 2003; Campbell et al., 2017; Rogers et al., 2017; Ruehr et al., 2023).

Land Surface Models (LSMs) are commonly used to simulate the carbon, water, and energy exchanges between the biosphere and the atmosphere, with a typical half-hour timestep (Fisher & Koven, 2020; Lawrence et al., 2019). In most LSMs, the algorithms for photosynthesis and leaf respiration are derived from equations designed to replicate the instantaneous responses recorded in laboratory or field measurements (Collatz et al., 1991; Farquhar et al., 1980; von Caemmerer & Farquhar, 1981). The maximum photosynthetic capacity (i.e., the catalytic activity of Rubisco for CO_2, V_{cmax}), for example, is treated such that it has a near-exponential response relationship to its value at 25°C ($V_{cmax,25}$), which is invariant (i.e., does not change with environmental conditions). This relationship reflects the initial response of enzymatic activity to environmental conditions (Bernacchi et al., 2003). The key physiological traits, such as $V_{cmax,25}$ and R_{25} (the basal leaf respiration rate at 25°C), are generally prescribed as constant parameters which differ between plant functional types (PFTs). Using historical observations as a baseline, each LSM calibrates a set of PFT-specific parameter values for $V_{cmax,25}$ and R_{25}. This allows different models to achieve a reasonable accuracy for the instantaneous response at the site scale (Bonan et al., 2003; Clark et al., 2011), but the calibration of multiple parameters together with model structures results in disagreement among LSMs in projections of the carbon cycle at regional or global scales, including disagreements even about the sign of the effect of global warming on primary production (Bonan & Doney, 2018; Fung et al., 2005). These differences between models have persisted for more than two decades (Arora et al., 2020; Friedlingstein et al., 2006; Li et al., 2015; VEMAP, 1995), and were identified as an urgent concern in the Intergovernmental Panel on Climate Change (IPCC) Sixth Assessment Report (Canadell et al., 2021).

A compelling body of evidence shows that these instantaneous responses of V_{cmax} and R_{canopy} are modified by the prevailing growth environment due to plant acclimation (Atkin & Tjoelker, 2003; Crous et al., 2022; Liang et al., 2013; Peng et al., 2019; Reich et al., 2016; Scafaro et al., 2017; Slot & Kitajima, 2015). $V_{cmax,25}$, for example, has been observed to acclimate to changes in temperature, consistently showing lower values under prolonged warming both in experiments and across spatial environmental gradients (Atkin et al., 2015; Crous et al., 2018; Kattge & Knorr, 2007; Kumarathunge et al., 2019; Scafaro et al., 2017; Smith & Dukes, 2017; Xu et al., 2021), and responding in a similar way to seasonal variations (i.e., lower values in the hotter season) (Crous et al., 2018; Jiang et al., 2020; Togashi et al., 2018). Down-regulation of $V_{cmax,25}$ would result in lower leaf respiratory ATP demand to maintain Rubisco turnover (Farquhar et al., 1980; Wang et al., 2020). Leaf respiration thus also shows thermal acclimation by down-regulation of R_{25} in response to increasing growth temperature spatially and temporally (Lee et al., 2005; Reich et al., 2016; Wang et al., 2020; Zhu et al., 2021). Compared to the authors' previous simulations using constant R_{25}, down-regulation of R_{25} coupled to $V_{cmax,25}$, in response to warming and increasing CO_2, halved the increase of R_{canopy} emission to the atmosphere during the past two decades (Ren et al., 2023).

Some studies have incorporated the acclimation of photosynthesis (Haverd et al., 2018; Oliver et al., 2022; Vuichard et al., 2019; Zhu et al., 2019) or leaf respiration (Butler et al., 2021; Huntingford et al., 2017), or both (Lombardozzi et al., 2015) into LSMs via various approaches. For example, a seasonal variation of $V_{cmax,25}$ is implemented into ORCHIDEE constrained by the leaf age effect (Krinner et al., 2005). An approach widely used in most well-known LSMs (e.g., JULES, CABLE, ELM, ORCHIDEE) is that $V_{cmax,25}$ (and/or R_{25}) acclimates to the daily average temperature during the past few days (T_{daily}), declining linearly with increasing T_{daily} according to an empirical function (Butler et al., 2021; Haverd et al., 2018; Huntingford et al., 2017; Vuichard et al., 2019). These LSMs then assign empirical, PFT-specific parameter values for the thermal acclimation rate. The use of T_{daily} to express R acclimation (Atkin et al., 2008; Huntingford et al., 2017) is not sufficient to capture the full

impact of growth temperature on leaf respiration, given different respiratory demands during night (for starch degradation and sucrose export) and day (for the regeneration of Rubisco) (Stitt & Schulze, 1994; Turnbull et al., 2002). Furthermore, the acclimation rate is affected by environmental effects other than temperature (Reich et al., 2021; Smith & Dukes, 2017; Wang et al., 2020), including atmospheric CO_2 concentration (Bagley et al., 2015; Sage et al., 1989; Tissue et al., 1993), radiation (Atkin et al., 1998; Ghannoum et al., 1997; Liu et al., 2024), and vapor pressure deficit (VPD) (Li et al., 2018; Middleby et al., 2024).

Recent studies have shown that eco-evolutionary optimality (EEO) theories are able to predict observed general patterns of trait variation with limited universal parameters, and can therefore provide parsimonious models of plant behavior (Franklin et al., 2020; Harrison et al., 2021). EEO theories incorporate the complex environmental effects with the assumption that plants acclimate to multiple environmental changes, whereby long-term average traits tend toward their optimum, allowing plants to maximize the carbon benefit (Harrison et al., 2021). EEO theories, for example, successfully predict global patterns in $V_{cmax,25}$ (Dong et al., 2022; Smith et al., 2019), and its seasonal variation (Jiang et al., 2020), and altitudinal trends in multiple traits related to photosynthesis (Peng et al., 2020; Xu et al., 2021). A universal productivity model (P model: Wang et al., 2017; Stocker et al., 2020) which incorporates two EEO hypotheses, specifically the coordination hypothesis (Maire et al., 2012) and the least cost hypothesis (Prentice et al., 2014), reproduces observed variations in GPP derived from flux towers globally when applied offline at the weekly to monthly time steps that approximate the time scale of acclimation with only two PFT-independent parameters (see details in Section 2.1.2) (Stocker et al., 2020). The P model has been shown to work also at a half-hourly time step by treating the instantaneous and acclimated timescales separately (Mengoli et al., 2022). A very recent study (Smith et al., 2024) has integrated the EEO-based treatment of photosynthetic acclimation into the land surface component of the Energy Exascale Earth System Model, to examine the effect of optimal photosynthetic acclimation on future ecosystem carbon storage. A second EEO-based hypothesis, that R_{25} acclimates to night-time temperature, in such a way as to support $V_{cmax,25}$ at a level which, in turn, acclimates to midday meteorological conditions following the coordination hypothesis, also predicts both the spatial and temporal patterns of variations in R_{25} with only one tunable parameter (Ren et al., 2023). Although these two increasingly well-understood principles provide a simple and robust way to incorporate photosynthesis and R_{canopy} acclimation, they have not been implemented together in a modeling framework.

In this study, we have implemented EEO-based schemes representing the acclimation of photosynthesis and leaf respiration in the Noah MP LSM (Niu et al., 2011; Yang et al., 2011), based on three EEO hypotheses: two key hypotheses incorporated in the P model (the coordination hypothesis, Maire et al. (2012) and the least cost hypothesis, Prentice et al. (2014)), and the V_{cmax}-R_{canopy} coupling hypothesis (Ren et al., 2023). We first compared the variations in $V_{cmax,25}$ and R_{25} between field measurements and simulations from the standard Noah MP scheme and the EEO-based scheme. We then compared the simulated GPP and R_{canopy} on half-hourly, monthly and annual time scales between the standard and EEO-based schemes. Finally, we investigated the responses of GPP and R_{canopy} to warming and CO_2 enhancement in both versions of the model.

2. Materials and Methods

We ran two sets of model experiments to simulate GPP and R_{canopy}: one with the standard Noah MP scheme and the other with the new EEO-based scheme. In Section 2.1, we summarize the general approach used in the standard Noah MP and introduce the EEO-based scheme. We then describe the experimental design (Section 2.2), the forcing and benchmark data (Section 2.3), the model evaluation (Section 2.4) and the sensitivity analyses (Section 2.5).

2.1. Model Description

2.1.1. Standard Noah MP Scheme

The standard version of Noah MP simulates the instantaneous photosynthetic rate for a single leaf (*PSN*) as the lesser of carboxylation-limiting rate rate (A_C, determined by V_{cmax}) and light-limiting rate (A_J, determined by light), that is: $PSN = \min(A_C, A_J)$, where A_C and A_J are given as follows (Collatz et al., 1998; Farquhar et al., 1980):

$$A_C = \begin{cases} V_{\text{cmax}} \cdot \dfrac{c_i - \Gamma^*}{c_i + K}, & \text{C3 plant} \\ V_{\text{cmax}}, & \text{C4 plant} \end{cases} \quad (1)$$

$$A_J = \begin{cases} \dfrac{J}{4} \cdot \dfrac{c_i - \Gamma^*}{c_i + 2\Gamma^*}, & \text{C3 plant} \\ \dfrac{J}{4}, & \text{C4 plant} \end{cases} \quad (2)$$

where V_{cmax} is the catalytic activity of Rubisco for carboxylation, c_{i} is the leaf-internal CO_2 partial pressure, Γ^* is the photorespiratory compensation point, K is the effective Michaelis–Menten coefficient of Rubisco, and J is the electron transport rate. Detailed information and equations of Γ^* and K are given in Tables S1 and S2 in Supporting Information S1.

The standard version of Noah MP simulates the instantaneous V_{cmax} from its basal value at leaf level ($V_{\text{cmax,25}}$) adjusted to account for foliage nitrogen content, soil moisture and temperature, derived from Collatz et al. (1991):

$$V_{\text{cmax}} = V_{\text{cmax,25}} \cdot N_e \cdot \beta \cdot f_v(T) \quad (3)$$

where $V_{\text{cmax,25}}$ is a constant value for each PFT provided in a look-up table (see Table S3 in Supporting Information S1), N_{e} (unitless) denotes the foliage nitrogen limitation factor from $V_{\text{cmax,25}}$ to V_{cmax}, given part of foliage nitrogen is invested in Rubisco (Peng et al., 2021; Walker et al., 2014). N_{e} is parameterized to be constant with a value of 2/3. β is the soil moisture limitation factor, and $f_v(T)$ represents the instantaneous temperature response (Table S2 in Supporting Information S1). There are three possible options (Noah type, CLM type and SSiB type) for quantifying the β factor in Noah MP (Niu et al., 2011), but here we use the Noah type following the recommendation from HRLDAS (https://github.com/NCAR/hrldas). β is parameterized by the Noah type as $\frac{\theta - \theta_{wp}}{\theta_{fc} - \theta_{wp}}$, where θ (m^3/m^3) is the soil moisture simulated from the "SOILWATER" module, and θ_{wp} (m^3/m^3) and θ_{fc} (m^3/m^3) represent respectively the soil moisture at wilting point and field capacity and are specified from soil texture (Niu et al., 2011).

In the standard scheme, c_{i} is obtained by numerical iteration based on the Ball-Berry model, which reflects the carbon-water coupling controlled by stomatal behavior (Ball et al., 1987). Most variables involved in Equations 1 and 2 are calculated for each iteration until c_{i} converges; following Niu et al. (2011) we use the default value of three iterations for convergence.

The absorbed photosynthetically active radiation (*aPAR*) and the intrinsic quantum efficiency of photosynthesis at 25°C (φ_{25}) jointly determine the rate of electron transport (J in Equation 2) with a conversion of 4.6 μmol J^{-1}(Meek et al., 1984; Niu et al., 2011) such that:

$$J = 4.6 \cdot \text{aPAR} \cdot \varphi_{25} \quad (4)$$

where φ_{25} is assumed to be 0.06 μmol CO_2/μmol photon for each PFT. The standard Noah MP is a two-leaf model, with separate calculations of aPAR for sunlit (aPAR_{sun}) and shaded (aPAR_{sha}) leaves. The average aPAR_{sun} and average aPAR_{sha} per leaf area are obtained from the "RADIATION" module based on the solar radiation input and two-stream radiative transfer equations (Niu et al., 2011). The average sunlit and shaded photosynthetic rates per leaf area (PSN_{sun}, PSN_{sha}) are calculated based on the average aPAR_{sun} and aPAR_{sha}, respectively.

The canopy photosynthesis rate (i.e., GPP) is then given as the sum of the sunlit and shaded rates (Sellers et al., 1992):

$$\text{GPP} = \text{PSN}_{\text{sha}} \cdot \text{LAI}_{\text{sha}} + \text{PSN}_{\text{sun}} \cdot \text{LAI}_{\text{sun}} \quad (5)$$

where LAI_{sha} and LAI_{sun} are the shaded and sunlit leaf area index (LAI) and vary over the diurnal cycle of solar zenith angle, obtained from the "RADIATION" module based on the LAI input. Although the standard Noah MP is usually run using prescribed LAI from a look-up table or using LAI as simulated by the dynamic vegetation module, it can also be run using LAI from other sources. To reduce the uncertainty due to the calculation of LAI, here we use satellite-derived LAI as input (Section 2.3).

The standard Noah MP scheme simulates R_{canopy} from its basal value at leaf level (R_{25}) modified by N_e, β, the effects of temperature ($f_r(T)$) and LAI (Niu et al., 2011) as:

$$R_{canopy} = R_{25} \cdot N_e \cdot \beta \cdot f_r(T) \cdot \mathrm{LAI} \tag{6}$$

where leaf-level R_{25} is constant for each PFT and given in a look-up table (see Table S3 in Supporting Information S1). $f_r(T)$ is originally adopted as the Q_{10} equation in the standard scheme; here we use a peaked temperature-dependent equation from Heskel et al. (2016) (Table S2 in Supporting Information S1) to reflect the non-linearity of the response of natural log transformed R_{canopy} to temperature. In addition to $V_{cmax,25}$ and R_{25}, there are up to 10 parameters related to each PFT used in the calculations of GPP and R_{canopy} (Table S4 in Supporting Information S1).

2.1.2. EEO-Based Scheme With Acclimation Processes

The EEO-based scheme adopts the same model as the standard Noah MP scheme (i.e., Equations 1 and 2) to simulate photosynthetic rate and uses Beer's law to account for the light exposure within the canopy. However, this new scheme follows the big-leaf paradigm and incorporates the acclimated traits ($V_{cmax,25}$, maximum J at 25°C ($J_{max,25}$), c_i and R_{25}) based on three EEO hypotheses: the coordination hypothesis (Maire et al., 2012), the least cost hypothesis (Prentice et al., 2014) and the V_{cmax}-R_{canopy} coupling hypothesis (Ren et al., 2023). Traits are updated at the daily timestep, acclimating to the average environmental conditions over the prior 15 days, which is plausible and consistent with the expected life-cycle of Rubisco (Mäkelä et al., 2008) and multi-site analysis (Mengoli et al., 2022).

The EEO-based scheme represents the light absorbed by the whole-canopy leaves (I_{abs}) as the product of the fraction of absorbed photosynthetically active radiation (f_{PAR}) and incident solar radiation (W m^{-2}) with a conversion factor of 2.04 μmol J^{-1} (Meek et al., 1984). This scheme assumes that J tends to a maximum value (J_{max}), limited by the regeneration of RuBP at high light levels (Stocker et al., 2020; Wang et al., 2017):

$$J = 4\varphi_0 I_{abs} / \sqrt{1 + \left(\frac{4\varphi_0 I_{abs}}{J_{max}}\right)^2} \tag{7}$$

where φ_0 is the intrinsic quantum efficiency of photosynthesis derived from an empirical temperature-dependent function (Bernacchi et al., 2003) (Table S2 in Supporting Information S1). Using whole-canopy J, J_{max} and V_{cmax}, the EEO-based scheme simulates half-hourly GPP as the minimum of two rates following Equations 1 and 2.

The canopy V_{cmax} and J_{max} at the instantaneous temperature (T_{ins}) are adjusted from the optimal $V_{cmax,25}$ and $J_{max,25}$ following the Arrhenius equations (f_v and f_j, see Table S2 in Supporting Information S1), respectively:

$$V_{cmax} = V_{cmax,25} \times f_v(T_{ins}) \tag{8a}$$

$$J_{max} = J_{max,25} \times f_j(T_{ins}) \tag{8b}$$

Optimal $V_{cmax,25}$ and $J_{max,25}$ are derived from the values at the acclimated temperature (T_{accl}) by inverting the Arrhenius equations:

$$V_{cmax,25} = V_{cmax,opt} \times f_v^{-1}(T_{accl}) \tag{9a}$$

$$J_{max,25} = J_{max,opt} \times f_j^{-1}(T_{accl}) \tag{9b}$$

here $V_{cmax,opt}$ and $J_{max,opt}$ represent the optimal V_{cmax} and J_{max} acclimated to the average midday (11:30–12:30 solar time) environmental conditions (to make full use of light) during the prior 15 days (Mengoli et al., 2022). T_{accl} is the average midday temperature over the past 15 days.

The canopy $V_{cmax,opt}$ and $J_{max,opt}$ are then predicted by the coordination hypothesis, which posits that V_{cmax} and J_{max} tend toward their optimal values such that $A_J \approx A_C$, allowing plants to make use of all the available light (Chen et al., 1993; Haxeltine & Prentice, 1996; Maire et al., 2012; Yamori et al., 2006). Using Equations 1, 2 and 7, if $A_J = A_C$ then:

$$V_{cmax,opt} = \varphi_0 I_{abs}\left[(c_i + K)/(c_i + 2\Gamma^*)\right]\beta\sqrt{\left\{1 - \left[c^*\frac{(c_i + 2\Gamma^*)}{(c_i - \Gamma^*)}\right]^{2/3}\right\}} \tag{10a}$$

$$J_{max,opt} = 4\varphi_0 I_{abs}\beta/\sqrt{1/\left\{1 - \left[c^*\frac{(c_i + 2\Gamma^*)}{(c_i - \Gamma^*)}\right]^{2/3}\right\} - 1} \tag{10b}$$

where c^* is a cost factor for electron transport capacity and has been estimated as 0.41 ± 0.112 from the observed J_{max}:V_{max} ratios (Wang et al., 2017). For C_4 plants, $V_{cmax,opt}$ and $J_{max,opt}$ are predicted by assuming that both $(c_i + K)/(c_i + 2\Gamma^*)$ and $(c_i + 2\Gamma^*)/(c_i - \Gamma^*)$ are close to unity (Scott & Smith, 2022), with φ_0 estimated following Cai and Prentice (2020) (Table S2 in Supporting Information S1). The least cost hypothesis predicts that the optimal c_i responses to the ambient CO_2 partial pressure (c_a), vapor pressure deficit (VPD), temperature and atmospheric pressure, allowing plants to minimize the required costs of carboxylation and transpiration to maintain the given assimilation rate (Prentice et al., 2014). Thus, c_i as a function of environment is written:

$$c_i = \frac{\xi c_a + \Gamma^*\sqrt{\mathrm{VPD}}}{\xi + \sqrt{\mathrm{VPD}}} \tag{11}$$

$$\xi = \sqrt{\frac{\gamma(K + \Gamma^*)}{1.6\eta^*}} \tag{12}$$

where ξ represents the sensitivity of the c_i: c_a ratio to VPD; the variation in this ratio as shown by leaf $\delta^{13}C$ measurements globally has been shown to be reliably predicted by the EEO formulation. γ denotes the ratio of carboxylation to transpiration cost factors at 25°C and has been estimated as 146 ± 2.7 based on the leaf $\delta^{13}C$ (Stocker et al., 2020). η^* is the viscosity of water relative to its value at 25°C; its detailed equation is shown in Table S2 in Supporting Information S1. All climatic variables used in Equations 11 and 12 to predict $V_{cmax,opt}$ and $J_{max,opt}$ are calculated as their midday averages over the past 15 days except for the instantaneous VPD and β (in order to account for the fast response of stomata to moisture changes) (Mengoli et al., 2022).

After predicting the canopy $V_{cmax,opt}$, the optimal canopy R_{25} is integrated into Noah MP based on the EEO hypothesis that leaf respiration evaluated at night-time temperature (T_{night}) is proportional to the acclimated V_{cmax} (Ren et al., 2023), thus optimal R_{25} is predicted as:

$$R_{25} = b\frac{V_{cmax,opt}}{f_{r(T_{night})}} \tag{13}$$

where b is estimated as 0.018 ± 0.0004 (mean ± S.D.) based on global measurements of R_{leaf} and V_{cmax} including a 5-year warming experiment, and an extensive field-measurement data set at ambient temperature (see details in Section 2.3.3). T_{night} is the average temperature during night-time (when the sun elevation was <0°, i.e. below the horizon) over the past 15 days, and f_r is a peaked temperature-dependent equation from Heskel et al. (2016) (Table S2 in Supporting Information S1). This scheme links R_{25} and V_{cmax} and therefore predicts the environmental impacts on R_{25} via V_{cmax}.

The EEO-based scheme therefore simulates half-hourly R_{canopy} from the canopy R_{25} following the temperature-dependent equation:

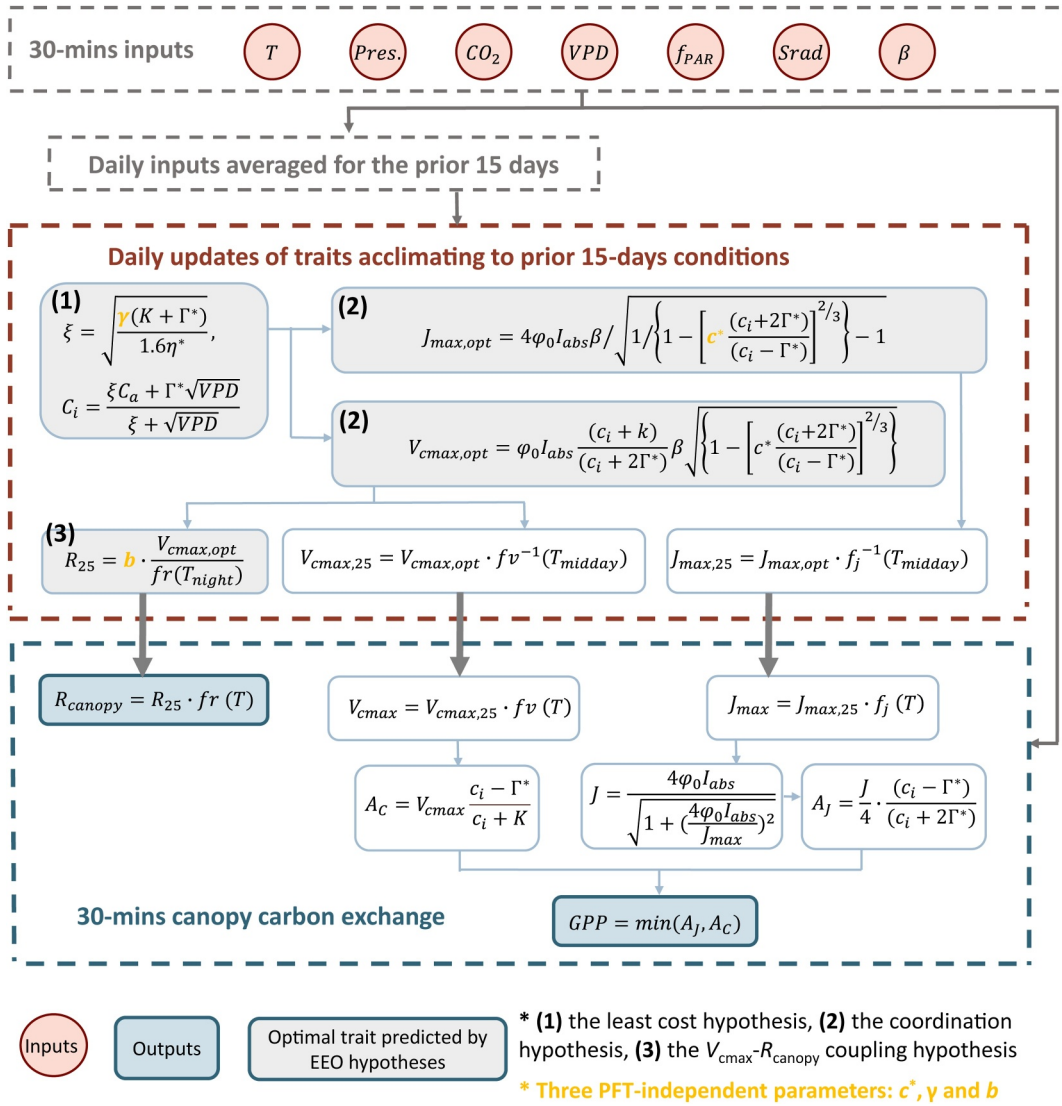

Figure 1. Flowchart of the trait-acclimation scheme incorporated in Noah MP. The inputs (shown in pink circle boxes) are air temperature (T), air pressure (*Pres.*), atmospheric CO_2 concentration (CO_2), vapor pressure deficit (VPD), solar radiation (*Srad*), the fraction of absorbed photosynthetically active radiation (f_{PAR}), and the soil moisture limitation factor (β). T_{midday} and T_{night} are the average midday and night-time (when the sun elevation was <0°) temperature over the prior 15 days, respectively. β is calculated using the same approach as in the standard scheme. The outputs (shown in the rectangle boxes) are 30-min GPP and R_{canopy}. Three EEO hypotheses are used to predict the optimal traits: the least cost hypothesis (c_i), the coordination hypothesis ($V_{\text{cmax,25}}$, $J_{\text{max,25}}$) and the V_{cmax}-R_{canopy} coupling hypothesis (R_{25}). The three tunable parameters ($c^* = 0.41 \pm 0.112$, $\gamma = 146 \pm 2.7$ and $b = 0.018 \pm 0.0004$) are shown in yellow font. This flowchart gives the equations for C_3 plant for illustrative purposes. The equations for C_4 plants are given in Methods. All parameters are described in Table S1 in Supporting Information S1 and their equations are given in Table S2 in Supporting Information S1.

$$R_{\text{canopy}} = b\frac{V_{\text{cmax,opt}}}{f_{r(T_{\text{night}})}} \times f_r(T_{\text{ins}}) \tag{14}$$

To avoid storing the antecedent forcing data, we apply the exponential moving average approach with the moving window of 15 days (Mengoli et al., 2022) to predict the optimal $V_{\text{cmax,25}}$, $J_{\text{max,25}}$ and R_{25} at the daily time step. The instantaneous V_{cmax}, J_{max} and R_{canopy} are then adjusted by the instantaneous temperature to simulate the half-hourly carbon flux.

Thus, the EEO-based scheme (Figure 1) incorporates the photosynthetic and leaf respiratory acclimation driven by temperature, radiation, VPD, atmospheric CO_2 concentration, soil moisture and atmospheric pressure (Figures S1 and S2 in Supporting Information S1), but only involves three tunable parameters (c*, γ and b) (Table S4 in Supporting Information S1), whose values have been estimated from data independent of the observations used for model evaluation.

2.2. Experimental Design

Both the standard and EEO-based experiments adopted the same physical parameterizations for other modules following the GLDAS options recommended by HRLDAS (see details in Table S5 in Supporting Information S1). To reduce the uncertainties derived from the initial conditions and equilibrate soil moisture and soil temperature, the two experiments were spun up for one loop according to the available site-years period at each site (ranging from 1 to 22 years, Tables S6 and S7 in Supporting Information S1), and then run at half-hourly time steps. Simulations at flux tower sites were driven by forcing from the FLUXNET2015 data set (Pastorello et al., 2020). Simulations at field trait-measurement sites were driven by forcing extracted from a global gridded data set (Section 2.3) during the appropriate period, and the simulated $V_{cmax,25}$ and R_{25} was obtained for the days when measurements were taken.

2.3. Data

2.3.1. Forcing Data

Both experiments were run using the same forcing. At individual flux sites, we used the half-hourly climate forcings from FLUXNET2015 (Pastorello et al., 2020, February 2020 updated version). The forcings are wind speed (u, m/s), air temperature (T, °C), relative humidity (RH, %), air pressure ($pres$., Pa), shortwave radiation ($Srad$, W/m^2), longwave radiation ($Lrad$, W/m^2), precipitation ($prec$., mm/30 min). For other sites where traits were measured, we extracted these climate forcings from the WATCH Forcing Data Methodology applied to ERA5 (WFDE5) global data set with a spatial resolution of 0.5°, hourly from 1979 to 2019 (Cucchi et al., 2022). We used the reprocessed MODIS LAI product, which has eliminated the effect of clouds (Yuan et al., 2011). This data set has a resolution of 0.04° and 8 days from 2001 to 2020. We extracted the LAI value for each flux and trait site and derived daily LAI by linear interpolation. The atmospheric CO_2 concentration was updated annually using its global annual average from the National Oceanic and Atmospheric Administration (NOAA; Lan et al., 2024).

2.3.2. Initialization Data

The initial state variables, specifically soil moisture, soil temperature, canopy water, snow water equivalent and snow depth, were obtained from the Global Land Data Assimilation System (GLDAS; Rodell et al., 2004). Location-related information including elevation, soil category, PFT (used in the standard scheme), and fraction of vegetation cover (FVC), were also prescribed. The elevation and vegetation type for each site were taken from FLUXNET2015. Soil type information was derived from the global soil data set for Earth system modeling (GSDE; Shangguan et al., 2014). FVC was taken from the global land surface satellite (GLASS) product (Jia et al., 2015).

2.3.3. Benchmark Data

We combined three existing data sets (Figure 2 and Table S6 in Supporting Information S1) to evaluate how well the models captured the spatial and temporal variations in $V_{cmax,25}$ and R_{25}: the Boreal Forest Warming at an Ecotone in Danger experiment (B4WarmED: Reich et al., 2021), the Leaf Carbon Exchange data set (LCE: Smith & Dukes, 2017), and the Global Leaf Respiration Database (GlobResp: Atkin et al., 2015). B4WarmED provided data on the seasonal variation in $V_{cmax,25}$ (994 samples) and R_{25} (1,600 samples) during growing seasons from 2009 to 2013, measured at ambient temperature and at 3.4°C above ambient temperature. The spatial variability in $V_{cmax,25}$ and R_{25} was evaluated using measurements at ambient temperature from the LCE and GlobResp data sets. All three data sets followed a similar measurement protocol: fully expanded leaves were taken in the morning and were measured in a darkened chamber after at least 10 min' dark adjustment. GlobResp provides R_{25} directly; LCE and B4WarmED provided measured leaf temperature, so instantaneous R (R_{ins}) at the measured temperature (T_{ins}) could be adjusted to the standard 25°C according to $R_{ins} = R_{25} \cdot f_r\,(T_{ins})$ (Heskel et al., 2016).

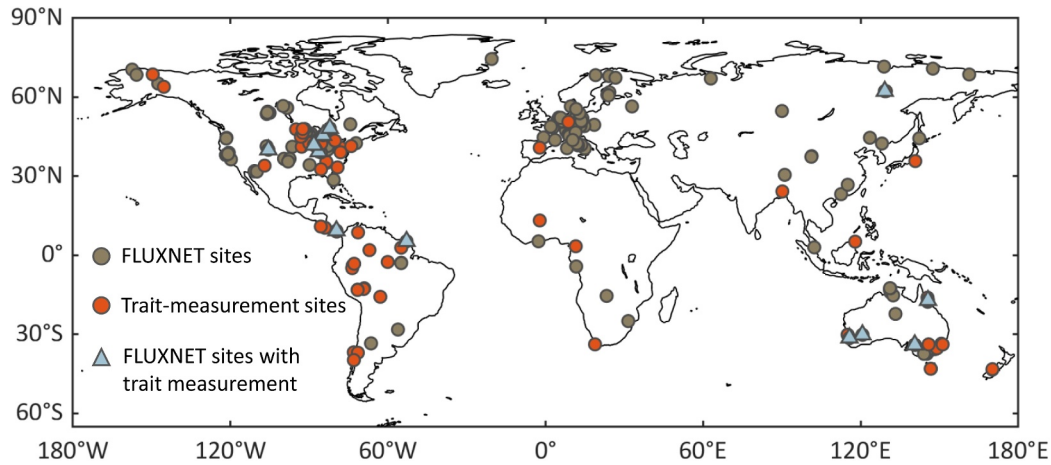

Figure 2. Locations of the 53 trait-measurement sites and the 168 selected FLUXNET sites. The red dots indicate the site locations where $V_{cmax,25}$ and R_{25} are measured derived from the combined data sets (B4WarmED, LCE and GlobResp). The gray dots indicate the FLUXNET site locations. The blue triangles show the 12 FLUXNET sites that have the measurements of $V_{cmax,25}$ and R_{25}.

After excluding samples with no specific measurement date, the data set compiled from B4WarmED, GlobResp and LCE provided a total of more than 3,000 paired measurements of $V_{cmax,25}$ and R_{25} covering 53 sites globally. Parameter b estimated from the B4WarmED warming samples was 0.019 ± 0.0003 (the yellow violin chart in Figure S3 in Supporting Information S1), which was very close to the value derived from the ambient samples (the purple violin charts in Figure S3 in Supporting Information S1). Thus, we used all samples from this combined data set to derive the factor b in *Eqn* 14 (0.018) as the mean ratio of measured R and V_{cmax}.

The EEO-based scheme predicted canopy level R_{25} under the big-leaf framework. This was then downscaled by LAI to derive the average leaf R_{25} (i.e., average leaf R_{25} = (whole-canopy) R_{25}/LAI) for comparison with the field measurements, since the field sampling likely reflects leaves developed at a range of irradiances at different levels in the canopy following Keenan and Niinemets (2016) and Dong et al. (2022). The leaf-level $V_{cmax,25}$ and R_{25} used in the standard Noah MP was also compared with these field measurements.We could not evaluate the acclimation of J_{max} in the EEO-based scheme, because of the limited number of field measurements available.

GPP estimated by the daytime partitionning method (GPP_DT_CUT_REF; Lasslop et al., 2010) from FLUXNET2015 was used to evaluate the simulated photosynthetic rate. We selected the FLUXNET2015 sites that provided the required variables and where the consistency in timeseries of gridded LAI and in-situ GPP (indicated by a correlation coefficient between the two time series >0.6, following Schober et al., 2018) showed that spatial representativeness of the satellite data and flux data are basically matched. The final data set consisted of 168 FLUXNET sites (Figure 2; Table S7 in Supporting Information S1) with over 1,200 site-years observations and covering 12 PFTs: croplands (CRO, 19 sites), closed shrublands (CSH, 3 sites), deciduous broadleaf forest (DBF, 25 sites), deciduous needleleaf forest (DNF, 1 site), evergreen broadleaf forest (EBF, 15 sites), evergreen needleleaf forest (ENF, 40 sites), grasslands (GRA, 25 sites), mixed forests (MF, 9 sites), open shrublands (OSH, 4 sites), savannas (SAV, 7 sites), wetlands (WET, 15 sites) and woody savannas (WSA, 5 sites). Since few field measurements separated R_{canopy} from total plant (or ecosystem) respiration, the benchmark of R_{canopy} was upscaled from single leaf measurement of R_{25} to canopy level: $R_{canopy} = \text{LAI} \cdot R_{25} \cdot f_r(T)$ with T representing 24-hr average temperature of the trait-measurement day. This estimation is acceptable because it derived a reasonable ratio of R_{canopy} to GPP (0.26, Figure S4 in Supporting Information S1), which was consistent with the previous studies (Reich et al., 2021; Wang et al., 2020). Twelve of the FLUXNET2015 sites also measured $V_{cmax,25}$, providing a benchmark to evaluate model performance in predicting traits and GPP.

2.4. Model Evaluation

We evaluated two aspects of model performance: the ability to capture (a) temporal and spatial variations in $V_{cmax,25}$ and R_{25} and (b) variations in GPP and R_{canopy}, using the metrics of r (correlation coefficient), R^2 (predictive ability), RMSE (root mean square error) and NSE (Nash-Sutcliffe Efficiency coefficient). We evaluated

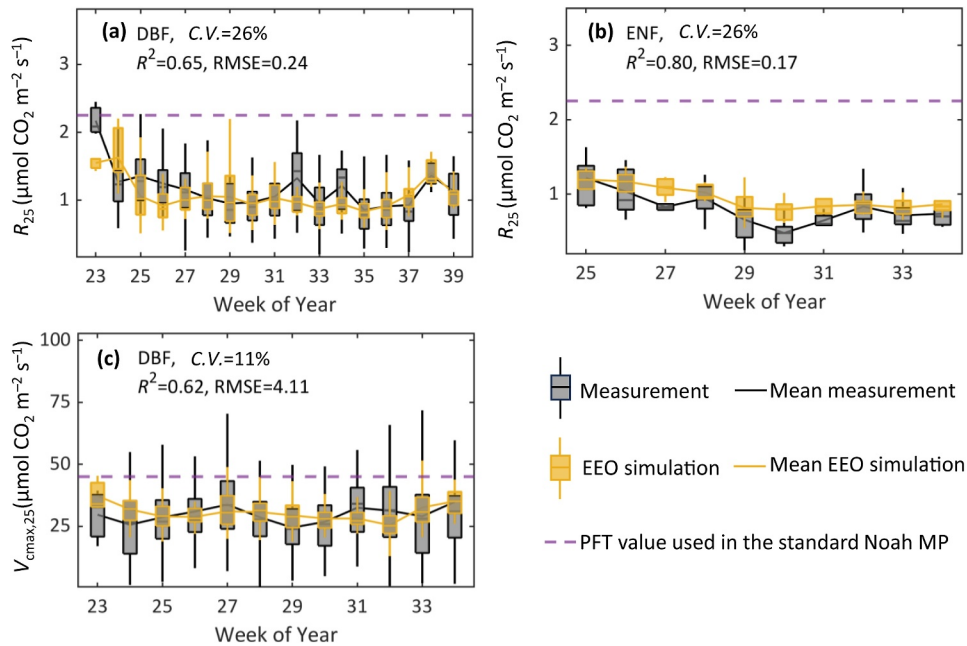

Figure 3. Temporal variations in R_{25} and $V_{cmax,25}$ for the specific PFT at B4WarmED site. The boxplots indicate the measured (gray box) and simulated by the EEO-based scheme (yellow box) trait values weekly averaged for 2009–2013 (25th percentile, 75th percentile and median; maximum and minimum for the whiskers). The black and yellow curves show the temporal variations in mean trait values for measurements and EEO-based simulations, respectively. The purple dotted line is the PFT parameter used in the standard version of Noah MP. R^2 and RMSE are calculated using the mean trait values. *C.V.* is the coefficient of variation of measured mean trait values. DBF: deciduous broadleaf forest; ENF: evergreen needleleaf forest. The seasonal variation of measured $V_{cmax,25}$ for ENF was not analyzed here due to the limited samplings.

the multi-year seasonal and spatial variations in $V_{cmax,25}$ and R_{25} for the two PFTs (DBF and ENF), that had the most measurements in the combined trait data set. We also compared the simulations to the half-hourly GPP and community averaged $V_{cmax,25}$ at the 12 FLUXNET sites from which these trait measurements were available. We then evaluated the simulated GPP across all the FLUXNET2015 sites on half-hourly, monthly, and annual scales. At the 53 trait-measurement sites, we also evaluated R_{canopy} from their temporal and spatial variations.

2.5. Parameter Uncertainty and Model Sensitivity Analysis

We conducted the uncertainty analysis of the three parameters involved in the EEO-predicted GPP and R_{canopy} using the standard error propagation formula. We analyzed the sensitivity of the simulated responses of GPP and R_{canopy} to warming and increasing CO_2 concentration in both model schemes, by changing temperature inputs by 1°C increments from 5°C to 35°C and atmospheric CO_2 concentration by 10 ppm increments from 380 ppm to 760 ppm. All other inputs were kept unchanged: LAI = 3, $\beta = 0.8$, $u = 2$ m/s, $RH = 70\%$, $pres.$ = 101.325 KPa, $Srad = 200$ W/m^2, $Lrad = 400$ W/m^2 and $prec.$ = 0.5 mm/30 min.

3. Results

3.1. Simulation of Trait Variations

Observed $V_{cmax,25}$ and R_{25} displayed substantial variability across seasons and latitudinal gradients within each vegetation type. The seasonal variability cannot be simulated in the standard Noah MP scheme because the values of $V_{cmax,25}$ and R_{25}, are specified by PFT (Figure 3) but both seasonal and latitudinal variations were reasonably well captured by the new EEO-based scheme (Figures 3 and 4). Specifically, multi-year weekly mean observations in R_{25} for DBF and ENF had clear seasonal patterns with highest R_{25} especially at the beginning and, to some degree, at the end of the growing season (*C.V.* ≈ 26%) (Figures 3a and 3b). Compared to R_{25}, the seasonal variation in $V_{cmax,25}$ derived from B4WarmED was less pronounced with a *C.V.* of 11% for DBF (Figure 3c). The EEO-based scheme reproduced the weekly average measurements, with R^2 of 0.73 for R_{25} and 0.62 for $V_{cmax,25}$, respectively. In addition to capturing the pattern of seasonal variation in $V_{cmax,25}$ and R_{25}, the EEO-based scheme

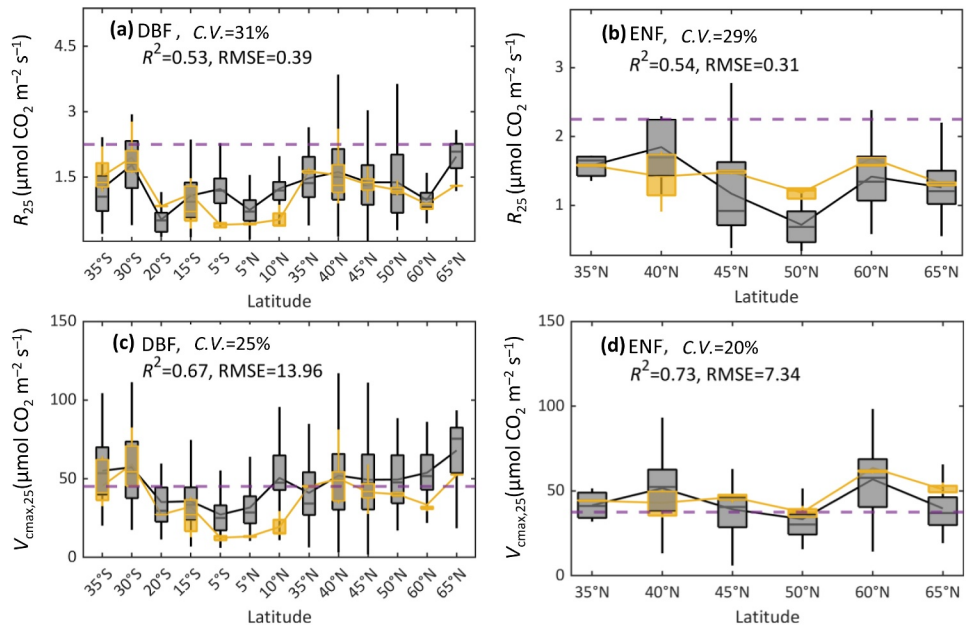

Figure 4. Spatial variations in R_{25} and $V_{cmax,25}$ for the GlobResp and LCE sites. The boxplots indicate the measured (gray box) and EEO simulated (yellow box) trait values for the 5° latitudinal bands (25th percentile, 75th percentile and median; maximum and minimum for the whiskers). The black and yellow curves show the spatial variations in mean trait values. The purple dotted line is the PFT parameter used in the standard scheme of Noah-MP. R^2 and RMSE are calculated for the mean trait values. *C.V.* is the coefficient of variation of measured mean trait values. This biome comparison is made by selecting the samples of deciduous broadleaf tree (figures a and c) or evergreen needleleaf tree (figures b and d) because the deciduous broadleaf forest (DBF) biome and the evergreen needleleaf forest (ENF) biome in the given latitudinal bands can include some other tree types.

also approximated the magnitude of those variables, whereas the standard scheme generally overpredicted both traits.

Observed R_{25} and $V_{cmax,25}$ showed strong variability within the same vegetation type across latitudinal bins (Figure 4), with higher values of both R_{25} and $V_{cmax,25}$ for communities growing in colder regions than those growing in warmer regions, with the spatial *C.V.* ranging from 20% to 31%. The measured R_{25} and $V_{cmax,25}$ for DBF at high latitudes (>60°N) were respectively 2.6 and 1.9 times larger than the values near the equator (5°N to 5°S) (Figures 4a and 4c). The standard scheme captured the observed $V_{cmax,25}$ of DBF (Figure 4c) reasonably well, but either overestimated (Figures 4a and 4b) or underestimated (Figure 4d) the observed range for the other cases. The standard scheme with constant parameter values cannot be expected to reproduce the observed seasonal variability. The EEO-based scheme underestimated R_{25} and $V_{cmax,25}$ for the equatorial bands, but predicted the magnitudes and the spatial variability in observed $V_{cmax,25}$ and R_{25} with R^2 of 0.7 and 0.54, respectively.

At all the FLUXNET2015 sites, EEO-simulated R_{25} and $V_{cmax,25}$ displayed strong variability across the seasonal climate range of any one biome (Figure 5). With the highest site-averaged latitude, the OSH sites had the strongest seasonal variability in traits among these biomes, with median *C.V.* of 51% for R_{25} and 53% for $V_{cmax,25}$. The WET, ENF, CRO, MF, GRA and DBF sites, which are concentrated between 40°N and 50°N and 40°S to 50°S of latitude, also had relatively strong seasonal variations with median *C.V.* ranging from 24% to 37%. EBF is the forest type with the least variability reflecting the relatively stable growing environment of tropical and subtropical EBF.

3.2. Evaluation of Carbon Flux Variations

The EEO-based scheme successfully reproduced the variations in half-hourly GPP at the 12 FLUXNET sites that provide field trait measurements (Figure 6). The EEO-based scheme improved the predictability of half-hourly GPP compared with the standard scheme during the period when the traits were measured, with the median R^2 for the 12 sites increasing from 0.86 (standard scheme) to 0.94 (EEO-based scheme) and median RMSE

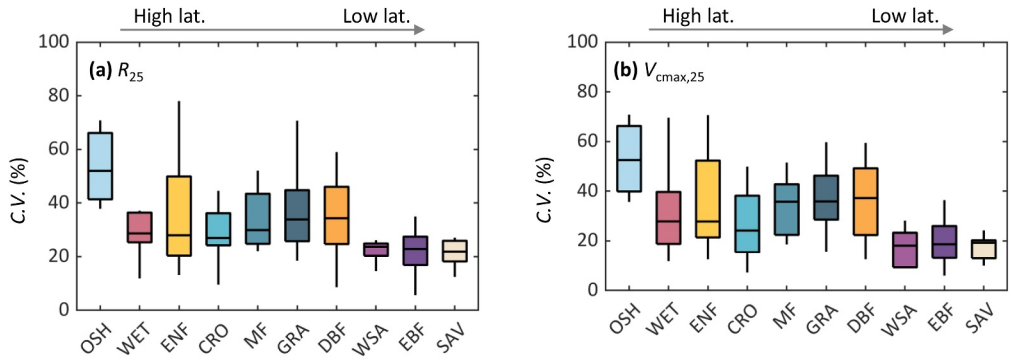

Figure 5. Coefficient of variation (*C.V.*) for the multi-year monthly average R_{25} and $V_{cmax,25}$ simulated by the EEO-based scheme at the FLUXNET sites. The boxplots indicate the *C.V.* for the sites within the same PFTs (25th percentile, 75th percentile and median; maximum and minimum for the whiskers). We only show the 10 PFTs for which there are data from at least three sites. The PFTs are ordered by the average site latitude of sites for that PFT.

decreasing from 3.6 (standard scheme) to 2.4 (EEO-based scheme) μmol CO_2 m^{-2} s^{-1} (Table S8 in Supporting Information S1). Improved performance was most noticeable at ENF (US-NR1), GRA (US-IB2), SAV (AU-Cpr, AU-GWW), and WSA (AU-Gin) sites. The standard scheme used a smaller $V_{cmax,25}$ than the in situ observations at US-NR1 site and this led to a 55% underestimation of GPP (RMSE = 5.3 μmol CO_2 m^{-2} s^{-1}); the EEO-based scheme underestimates GPP by only 4% (RMSE = 1.4 μmol CO_2 m^{-2} s^{-1}). The discrepancies between the observed and simulated GPP at the SAV and WSA sites were also smaller in the simulation using the EEO-based scheme, with the average RMSE decreasing from 2.1 (standard scheme) to 0.5 (EEO-based scheme) μmol CO_2 m^{-2} s^{-1}. Both schemes provided good representations of the sub-daily variations in GPP at the five boreal sites, although the EEO-based scheme was slightly better (site-averaged RMSE from 3.1 to 2 μmol CO_2 m^{-2} s^{-1}). The tower-derived GPP in 2014 at the CA-Gro site was much lower than the simulations and, indeed, the multi-year tower average (Figure S5 in Supporting Information S1). However, the satellite-derived LAI in 2014 at this site was not lower than the multi-year average. Consistent with the satellite LAI, the ground measured gcc (green chromatic coordinate) from Seyednasrollah et al. (2019) also did not show low values for the years with anomalously low GPP (i.e., 2014) (Figure S6 in Supporting Information S1). The discrepancy between flux-tower and simulated GPP could also reflect the impact of the extreme cold anomaly experienced at the site during the 2013/14 winter (Anderson & Gough, 2017), which inhibited the photosynthetic capacity of leaves. Indeed, the discrepancies between the simulated and tower-derived GPP in 2013 were smaller than that of 2014 (RMSE = 4.4 vs. 12.1 μmol CO_2 m^{-2} s^{-1}) (Figure S7 in Supporting Information S1). The tower-derived GPP at the RU-SkP site, which has the smallest average precipitation (no more than 1 mm day^{-1}, Figure S8 in Supporting Information S1) of the 12 sites, decreased significantly after 10 a.m. (Figure 6). We suspect the decrease in GPP is a result of stomatal closure in response to rising VPD during the midday period; this can be exacerbated in arid regions where low soil moisture may increase the sensitivity of stomata to VPD. This phenomenon was not captured by either scheme due to the empirical soil moisture limitation factor (β in Section 2.1) used in both.

The EEO-based scheme performed better than the standard scheme in predicting GPP variations at the half-hourly, monthly, and annual scales across all the FLUXNET2015 sites (Figure 7). The standard scheme generated a large spread in r across sites (0.79 ± 0.16, mean ± S.D.) for the half-hourly GPP (Figures 7a and 7b), whereas the EEO-based scheme had a more constrained distribution with an r of 0.84 ± 0.1. The standard scheme underestimated the monthly GPP by 10% especially for the high values with the fitted slope of 0.71 (Figure 7c), which was improved to 0.88 using the EEO-based scheme (Figure 7d). The EEO-predicted GPP was in good agreement with the observations in terms of the variation in the multi-year average GPP (Figures 7e and 7f) with a fitted slope of 0.95, with an increased R^2 (0.57 to 0.66) and NSE (0.54 to 0.62) compared to the standard scheme, and a decreased RMSE (173.75 to 145.35 μmol CO_2 m^{-2} s^{-1}).

The standard scheme overestimated measured R_{canopy} by more than twice, but the EEO-based scheme captured both the overall magnitude and the variability in R_{canopy} (Figure 8). Because of the overestimation of R_{25} (Figures 3a and 3b), the standard scheme produced an excessive CO_2 release from leaf respiration—generally twice that observed and nearly three times higher in ENF. The standard scheme showed stronger seasonal and

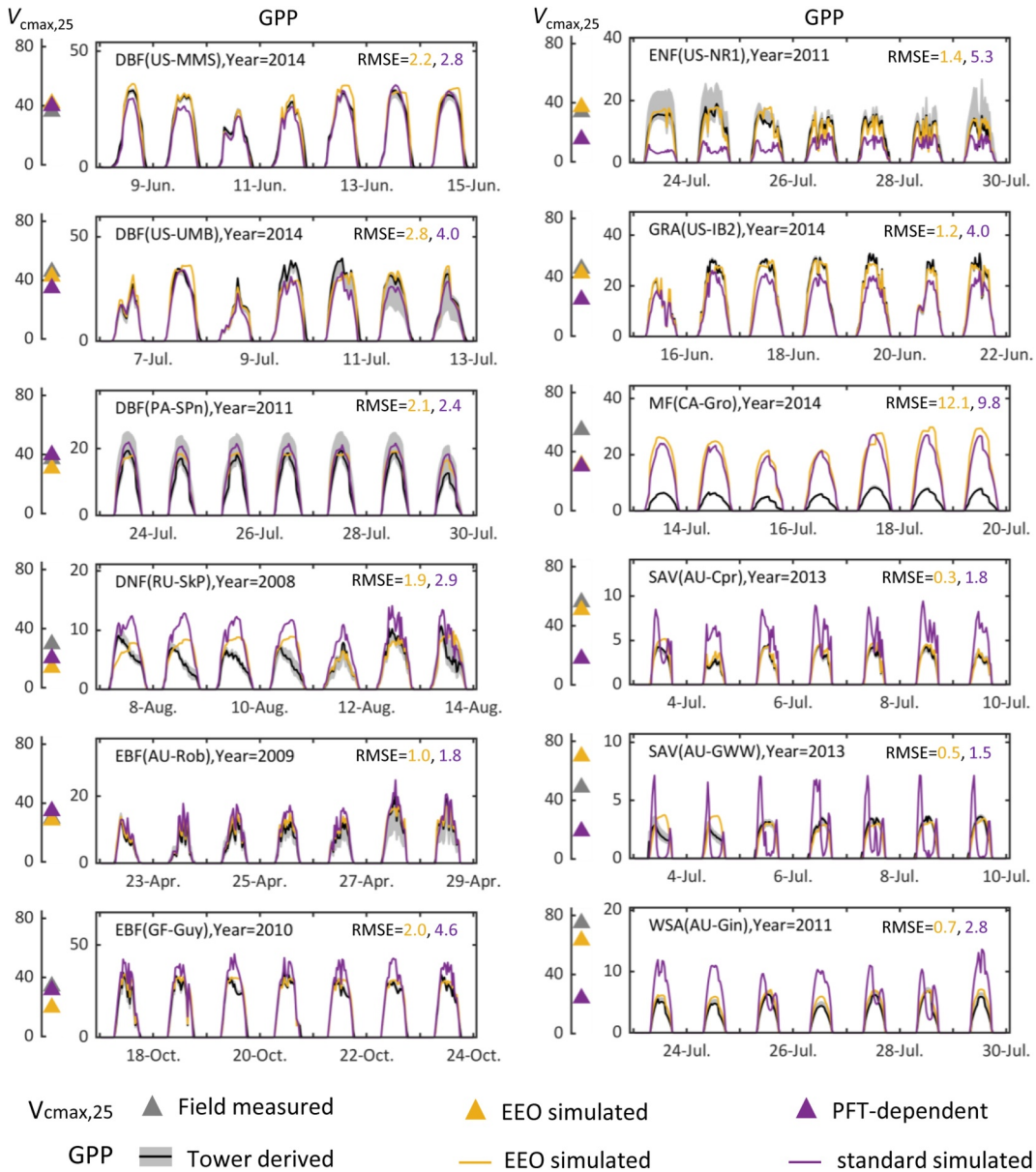

Figure 6. Half-hourly GPP at 12 FLUXNET sites at which field traits were measured. The left panel shows the mean $V_{cmax,25}$ during the field-measurement periods. The right panel shows the half-hourly GPP for the week covering the field-measurement periods. The gray shaded area in the right panel represents the uncertainty in tower-derived GPP calculated by the daytime partitioning method in the FLUXNET2015 data set. RMSE of GPP derived from the EEO simulation and standard simulation of each panel are shown as yellow and purple numbers, respectively.

spatial fluctuations in R_{canopy} than the observations (with $R^2 = 0.25$ for ENF, Figure 8b) due to the use of constant R_{25} across seasons and latitudinal gradients. The EEO-based scheme produced a more accurate R_{canopy}, with a maximum bias of 10%. The averaged RMSE for the EEO-based scheme was only 0.4 μmol CO_2 m^{-2} s^{-1}, less than one-fifth of RMSE of the standard scheme (2.2 μmol CO_2 m^{-2} s^{-1}). Overall, the EEO-based scheme captured the seasonal and spatial fluctuations in R_{canopy} ($R^2 = 0.77$ and 0.92, respectively) based on its acclimated R_{25}.

3.3. Responses of GPP and R_{canopy} to Warming and Increasing CO_2

The EEO-based scheme accounting for acclimation showed more moderate responses than the standard scheme to warming and atmospheric CO_2 enhancement (Figures 9a and 9c). With the temperature increasing from 5°C to the

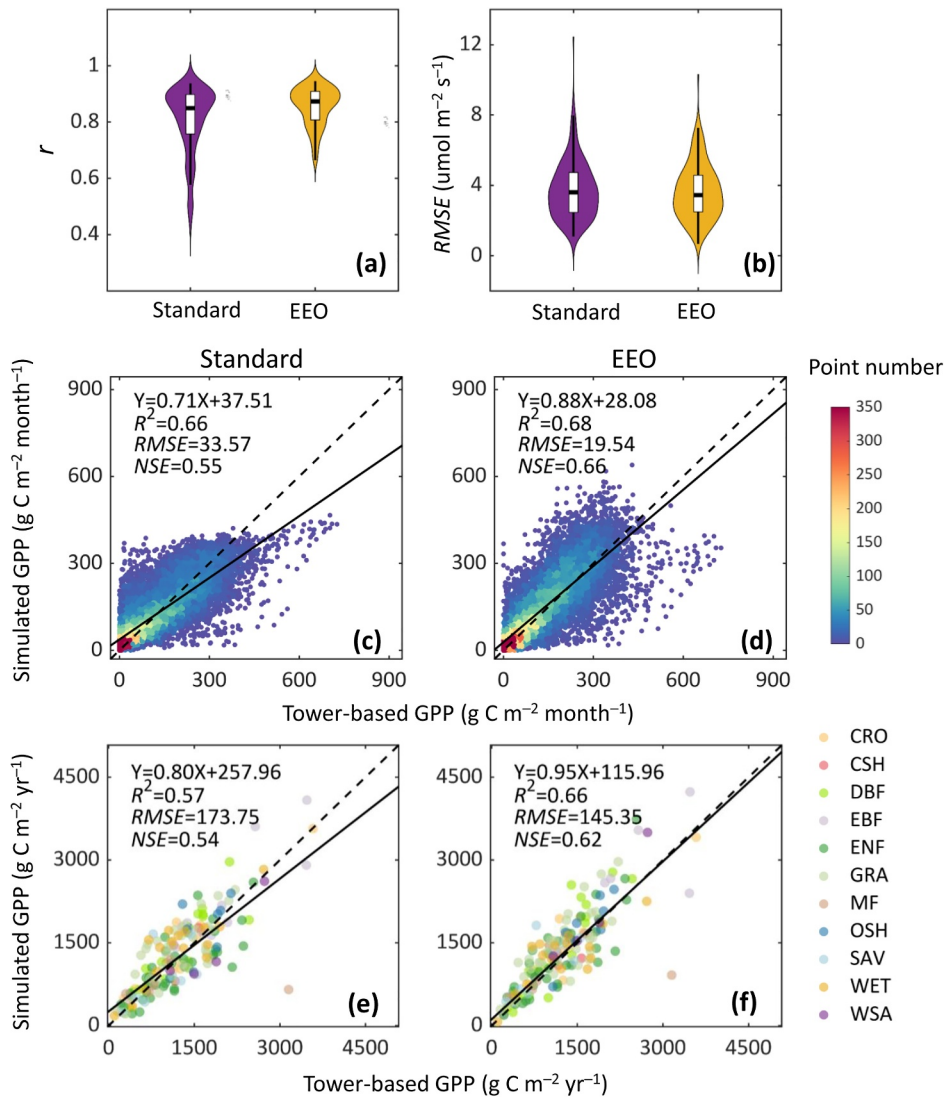

Figure 7. Evaluations of GPP for all FLUXNET sites at half-hourly, monthly, and annual scales. (a–b) *r* and RMSE of half-hourly tower-based and simulated GPP at 168 sites. The boxplot indicates the 25th percentile, 75th percentile and median among 168 sites, with maximum and minimum for the whiskers. (c–f) Scatter plots of monthly and annual GPP. The dashed and solid lines indicate the 1:1 ratio line and fitted line, respectively. NSE is the Nash-Sutcliffe efficiency coefficient.

temperature at which the peaked GPP occurred (T_{opt}), the EEO-based scheme showed a shallow rise of 17% in GPP (at the given 380 ppm) (Figure 9a and Figure S9a in Supporting Information S1). A much stronger response to warming was simulated by the standard scheme, with a larger GPP increase of 42% from 5°C to its T_{opt} (Figure 9b and Figure S9a in Supporting Information S1). The EEO-based scheme predicted a 10% increase in GPP (at the T = 5°C condition) under doubled CO_2 whereas the standard scheme produced a slightly larger increase of 12% (Figures 9a and 9b and Figure S9a in Supporting Information S1). The EEO-based T_{opt} increased from 16 to 19°C with a doubling of CO_2 concentration with a sensitivity of 0.14°C/10 ppm; the sensitivity of the standard scheme was 0.11°C/10 ppm but with a higher T_{opt} under the same CO_2 concentration level (Figures 9a and 9b).

The EEO-based scheme also showed a more moderate response of R_{canopy} to warming than the standard scheme (Figures 9c and 9d). The standard scheme predicted an increase in R_{canopy} five times greater than the EEO-based scheme with an increase of T from 5°C to 35°C (Figures 9c and 9d). Due to the reduction in predicted R_{25} with elevated CO_2 concentration (Figure S2 in Supporting Information S1), the EEO-based simulated R_{canopy} declined

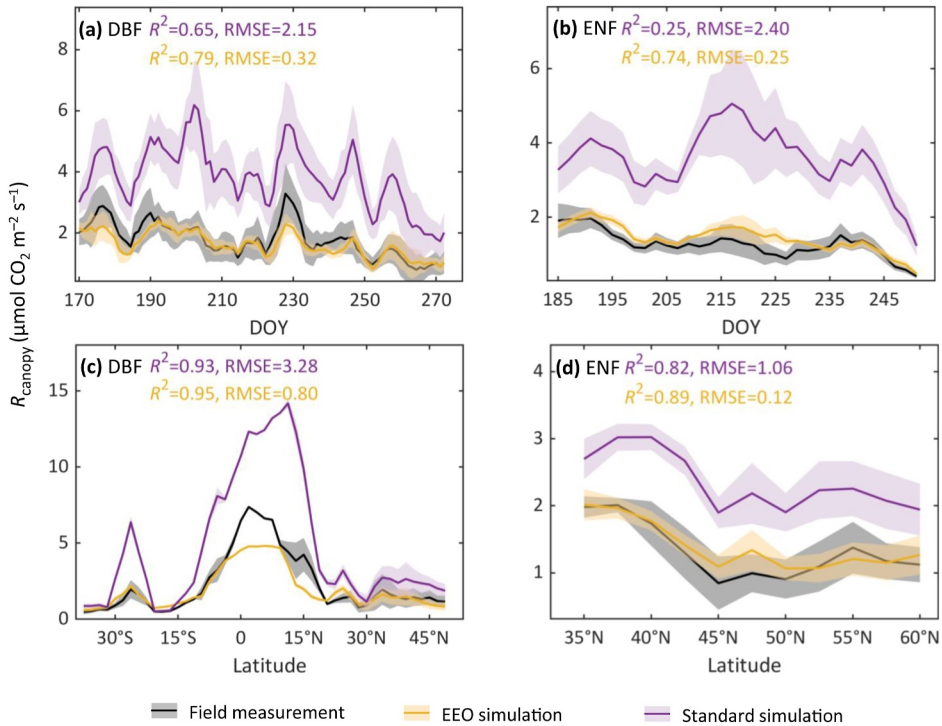

Figure 8. Evaluations of R_{canopy} at the trait-measurement sites. The solid curves show the variations in mean R_{canopy} with shaded area showing the mean ± S.D. The different colors indicate the R_{canopy} simulated by R_{25} using field observations (black), EEO simulations (yellow), and standard PFT parameters (purple), respectively. The mean R_{canopy} is the average of all species on the same day for 2009 and 2013 (a–b) or at the same latitude (c–d). R^2 and RMSE are based on the mean values with yellow and purple label for EEO and standard simulations, respectively.

with the sensitivity of −4%/10 ppm, whereas the standard scheme predicted a stable R_{canopy} under changing CO_2 concentration (Figure 9d and Figure S9b in Supporting Information S1).

4. Discussion

4.1. Improved Performance of the EEO-Based Scheme for GPP and R_{canopy}

The standard Noah MP scheme cannot produce the responses of V_{cmax25} and R_{25} to environmental changes whereas the EEO-based scheme allows for environmentally determined responses (Figures S1 and S2 in Supporting Information S1). Coupled with the optimal $V_{cmax,25}$, EEO-based R_{25} showed a negative response to increasing temperature (Figure S2a in Supporting Information S1) with a sensitivity of −4.2% $°C^{-1}$, close to the value (−4.4% $°C^{-1}$) derived from measurements across more than 100 sites (Wang et al., 2020). Increasing VPD is expected to have a positive impact on R_{25}, due to higher $V_{cmax,25}$ accompanying higher VPD (Smith et al., 2019). As predicted by the least-cost hypothesis, under higher VPD, plants tend to increase investment in Rubisco to compensate for the lower CO_2 supply induced by stomatal closure (Prentice et al., 2014). Relatively few studies have analyzed the effect of VPD; and results have been inconsistent. Zhu et al. (2021) observed increasing R_{25} under higher VPD, consistent with our results, but Reich et al. (2021) showed that R_{25} decreased with increased VPD probably because the respiratory substrate is reduced due to the decrease in net photosynthetic rate under higher VPD. Different water-use strategies (i.e., isohydric/anisohydric) (Zhao et al., 2023) could also impact the responses of photosynthesis and respiration. This could be taken into account in future by modifying the cost term used in the EEO formulations. R_{25} and $V_{cmax,25}$ increased in response to the lower air pressure at higher elevation (Figures S1f and S2f in Supporting Information S1) to compensate for the lower CO_2 supply, a finding that is consistent with observations along elevation transects (Bahar et al., 2017; Peng et al., 2020; Xu et al., 2021).

The EEO-based scheme, without any PFT-specific parameters, captured 62% of the temporal and 70% of the spatial variations in field measured $V_{cmax,25}$ (73% and 54% for R_{25}) (Figures 3 and 4). All leaf-level samples at a

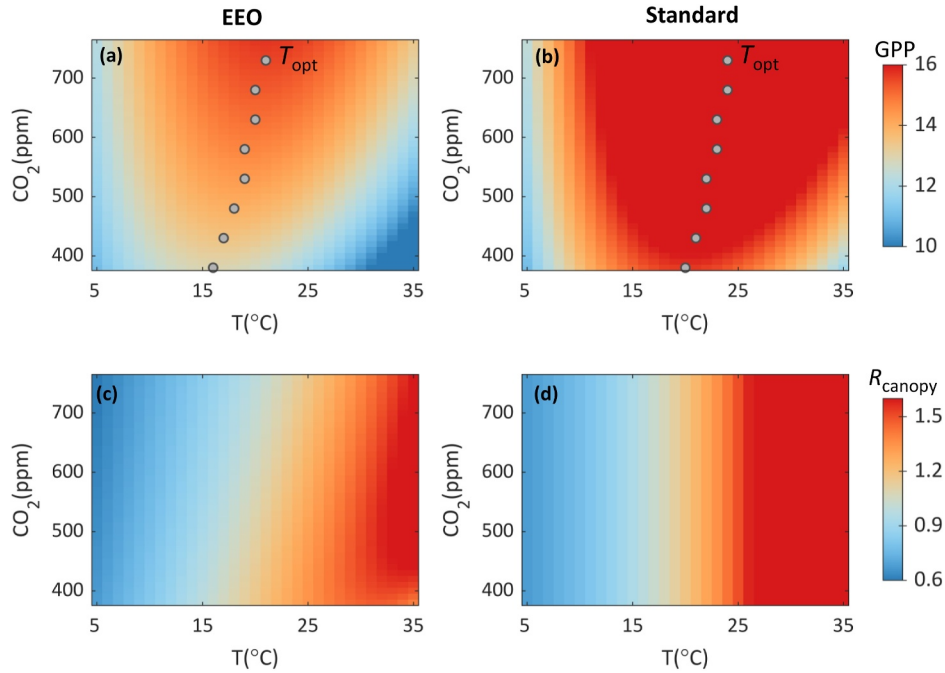

Figure 9. Responses of GPP and R_{canopy} to warming and increasing CO_2 simulated by the EEO-based (left panel) and standard (right panel) schemes. The unit of GPP and R_{canopy} is μmol CO_2 m^{-2} s^{-1}. T_{opt} indicated by the gray points (Figure a and b) is the corresponding temperature at the peaked GPP under a given CO_2 level. The standard-scheme simulations (S_{stan}) are re-scaled using the difference between EEO-scheme simulation (S_{EEO_0}) and standard-scheme simulation (S_{stan_0}) at 5°C and 380 ppm: re-scaled $S_{stan} = S_{stan} + S_{EEO\_0} - S_{stan\_0}$. This rescaling ensures that, the difference in response between the EEO and standard schemes is only affected by whether acclimation is considered or not, rather than model structure (i.e., big-leaf or two-leaf model).

given site were averaged to the community level, but there may still be some differences in how well these community averages represent predicted traits using site-averaged forcings because they do not necessarily include samples from all the plants at the site. This might cause some uncertainty in the evaluation results. However, our EEO-predicted $V_{cmax,25}$ was also consistent with the $V_{cmax,25}$ inversions derived from the FLUXNET2015 data set (Wang et al., 2022), which suggested strong temporal variability in $V_{cmax,25}$ cross sites with averaged *C.V.* exceeding 20%.

The standard version of Noah MP underestimated the observed magnitude of $V_{cmax,25}$ for the latitudinal bands >20°S or >35°N (Figure 4c), where more than 80% of the sites used for evaluation are located, resulting in a 10% underestimation of GPP compared to the monthly observations (Figure 7c). A similar underestimation of GPP has been found in most of the process-based biophysical models used in the TRENDY project (Sitch et al., 2015). The performance of the EEO-based model in explaining the observed monthly GPP ($R^2 = 0.68$, Figure 7d) is as good as or better than complex process-based, PFT-dependent models (R^2 ranging from 0.55 to 0.71: Zheng et al., 2020).

Consistent with the life-cycle of Rubisco and the acclimation time scale from physiological expectations (Mäkelä et al., 2008), empirical analyses over time and experimental manipulation (Reich et al., 2016, 2021), and multi-sites analysis (Mengoli et al., 2022), optimal traits are predicted by the EEO scheme using 15 days as their acclimation time scale in this study. Adjusting to the annual averaged environment conditions, GPP and R_{canopy} predicted by the EEO scheme (Figures S10 and S11 in Supporting Information S1) were still closer to the observations than the values predicted by the standard scheme (Figures 7 and 8), but not as good as the EEO predictions using optimal 15-day averaged traits (Figures 7 and 8). The EEO scheme adjusted to annual conditions overestimated R_{canopy} for ENF with RMSE of 1.06 μmol CO_2 m^{-2} s^{-1}, which was much larger than that adjusted to the prior 15-day averages (Figure S11d in Supporting Information S1). These results suggest that intra-annual trait variations are important for accurate prediction of GPP and R_{canopy}. It would also be worth

exploring whether the acclimation time scale is different for different environmental factors, if sufficient data were available from manipulation experiment.

4.2. Implications of Acclimation for the Global Carbon Cycle

Previous model studies have shown a positive carbon-climate feedback because the instantaneous temperature response of respiration is steeper than that of photosynthesis (Bonan & Levis, 2010; He et al., 2018; Krinner et al., 2005; Niu et al., 2011). Our findings imply that thermal acclimation of photosynthesis and leaf respiration leads to more CO_2 uptake (Figure 9), and thus reduces the positive carbon-climate feedback. This is consistent with field measurements that indicate plants assimilate more CO_2 with warming, as they can achieve the same function with fewer enzymes at higher temperature, thus reducing the respiratory loss incurred in maintaining catalytic capacity (Collalti et al., 2020; Luo et al., 2009; Wang et al., 2019). In our experiments, the increase of our acclimated R_{canopy} with warming was 12% lower than the non-acclimated response (Figure 9). Nevertheless, there are observations that indicate decreased plant carbon uptake under higher temperature, where warming-induced drought reduced ecosystem productivity (Ciais et al., 2005; Das et al., 2023; Wang et al., 2016; Zhao & Running, 2010), or increased wildfires increased carbon release (Mack et al., 2011; Mekonnen et al., 2019; Virkkala et al., 2024; Wang et al., 2021). Thus, the impact of warming is likely to be modulated by other environmental changes.

Our results also show increased atmospheric CO_2 concentration leads to an additional reduction of R_{25} (Figure S2d in Supporting Information S1), such that a doubling of the CO_2 concentration caused a 24% reduction in R_{canopy} (Figure 9c and Figure S8b in Supporting Information S1). This reflects the lower R_{25} and $V_{cmax,25}$ (Figures S1d and S2d in Supporting Information S1) due to the decreasing investment in Rubisco under higher CO_2 supply (Prentice et al., 2014; Smith et al., 2019). This effect has been diagnosed as the main driver of the temporal variation in global R_{canopy} over the past two decades (Ren et al., 2023).

4.3. Uncertainties and Limitations of This Study

Our results show the value of adopting a scheme that accounts for both R_{25} and $V_{cmax,25}$ acclimation under persistent warming and increasing CO_2 in terms of correctly predicting the carbon-climate feedback. However, there are two sources of uncertainty in the EEO predictions: the input data (LAI) and the model (model parameters). The MODIS LAI used here likely underestimates LAI, particularly in tropical regions, due to reflectance saturation at high leaf area (Gao et al., 2023). Comparisons with measured LAI at two tropical forest sites (BR-Sa1, GH-Ank) show that MODIS LAI is respectively 20% and 50% lower (Figure S12 in Supporting Information S1), measurements from Doughty & Goulden, 2008; Zhang-Zheng et al., 2024. EEO scheme predicted GPP at BR-Sa1 is 12.44 μmol CO_2 m^{-2} s^{-1}, which is 87% of the observed GPP; the EEO-predicted GPP at GH-Ank is about 60% of the flux tower observation, broadly consistent with the impact of saturation on the forcing data. LAI products inverted from lidar measurements (Ma et al., 2022) are expected to provide more accurate LAI inputs by addressing reflectance saturation at high leaf area, but currently only have limited availability. The difficulties and costs of LAI measurement on the ground, means that accurate prognostic LAI predictions would be useful for global carbon cycle modeling (Zhu et al., 2023), especially for past and future periods when there are no LAI observations. Our analysis of the impact of uncertainties in the estimates of parameters c^*, b and γ (Figure S13 in Supporting Information S1) showed that b and γ had negligible effects on the simulated GPP and R_{canopy}. However, the uncertainties associated with c^* are larger (~20%), consistent with findings of Qiao et al. (2020). This suggests that more attention is needed to constrain this parameter in the future to improve EEO predictions.

Limited by our understanding, three issues are not considered here. First, we used a fixed sensitivity of the intrinsic quantum efficiency (φ_0) to temperature, although this is known to vary with environmental conditions (Marečková et al., 2019; Sandoval et al., 2023; Zhang et al., 2024). A recent work (Huo et al., 2024) implemented the varying sensitivity of φ_0 to temperature in CLM model based on in situ observations collected at a site (71.28°N, 156.65°W). But a more complete understanding is required at global scale and a further understanding of the relationship with soil moisture limitation is also necessary to avoid parameterizing the uncertainty of one to the other (Sandoval et al., 2023). Second, we used Beer's law and assumed a similar decrease in $V_{cmax,25}$ and R_{25} with light exposure through the canopy. A limited number of field measurements suggest that the ratio between R_{25} and $V_{cmax,25}$ is lower near the ground than at the top of the canopy (Lamour et al., 2023; Weerasinghe

et al., 2014). More field measurements would be helpful to characterize this within-canopy gradient in future work. More importantly, we have not considered fine roots and stem respiration, or heterotrophic respiration, which could also impact ecosystem respiration (Chen et al., 2023). It would be worth exploring the full range of respiration processes in the future work to provide a more comprehensive basis for the assessment of feedbacks in the global carbon cycle.

5. Conclusions

We have tested an EEO-based scheme to represent the acclimation of photosynthesis and leaf respiration in the Noah MP LSM. We have shown that this scheme produces more realistic simulations of GPP and R_{canopy}, which are underestimated and overestimated respectively in the standard scheme. The EEO-based scheme also predicts the spatial and temporal variations in these two traits at different time scales across a range of different biomes more reliably than the standard scheme. Yet the new scheme has only three PFT-independent parameters, representing a considerable reduction in the number of parameters that must be specified (for each PFT) in the standard scheme. The new scheme is also less computationally demanding as it avoid the need for iterative solutions.

Data Availability Statement

The WFDE5 climate data set can be obtained from Cucchi et al., 2022 via 10.24381/cds.20d54e34. The atmospheric CO_2 concentration is available from Lan et al., 2024 via https://doi.org/10.15138/9N0H-ZH07. The GLDAS data set to initialize model is downloaded from Beaudoing & Rodell, 2020 via 10.5067/SXAVCZFAQLNO. The GSDE data set to obtain the soil texture is available from Shangguan et al., 2014 via 10.11888/Soil.tpdc.270578. The GlobResp data set can be obtained from the Plant Trait Database (TRY) (https://www.try-db.org/TryWeb/Data.php). The LCE data set is available in the Supporting Information of Smith and Dukes (2017). The B4WarmED data set is from Reich et al. (2021). FLUXNET2015 can be downloaded from https://fluxnet.org/data/fluxnet2015-dataset. The code of the NoahMP-EEO model are publicly available from YanghangRen (2025) via zenodo (https://doi.org/10.5281/zenodo.14674455).

Acknowledgments

We thank three anonymous reviewers and editor for their helpful comments on earlier versions of this manuscript. This work was supported by National Natural Science Foundation of China (72140005), the National Key Research and Development Program of China (2023YFF1305500), Sustainable Development International Cooperation Program of National Science Foundation of China (42361144875), Hainan Institute of National Park Research Program (KY-23ZK01), and Tsinghua University Initiative Scientific Research Program 20223080041. Participation of ICP and SPH has been supported by the High-End Foreign Expert programme of the China State Administration of Foreign Expert Affairs at Tsinghua University (H20240859). This research received support through Schmidt Sciences, LLC (YR, HW, SHP, ICP, GM). ICP also acknowledges support from the European Research Council (787203 REALM) under the European Union's Horizon 2020 research programme. PBR acknowledges support from the U.S. Department of Energy; Office of Science, and Office of Biological and Environmental Research award number DE-FG02-07ER644456; and the NSF Biological Integration Institute program (NSF-DBI 2021898).

References

Anav, A., Friedlingstein, P., Beer, C., Ciais, P., Harper, A., Jones, C., et al. (2015). Spatiotemporal patterns of terrestrial gross primary production: A review. *Reviews of Geophysics*, *53*(3), 785–818. https://doi.org/10.1002/2015RG000483

Anderson, C. I., & Gough, W. A. (2017). Evolution of winter temperature in Toronto, Ontario, Canada: A case study of winters 2013/14 and 2014/15. *Journal of Climate*, *30*(14), 5361–5376. https://doi.org/10.1175/JCLI-D-16-0562.1

Arneth, A., Harrison, S. P., Zaehle, S., Tsigaridis, K., Menon, S., Bartlein, P. J., et al. (2010). Terrestrial biogeochemical feedbacks in the climate system. *Nature Geoscience*, *3*(8), 525–532. https://doi.org/10.1038/ngeo905

Arora, V. K., Katavouta, A., Williams, R. G., Jones, C. D., Brovkin, V., Friedlingstein, P., et al. (2020). Carbon concentration and carbon climate feedbacks in CMIP6 models and their comparison to CMIP5 models. *Biogeosciences*, *17*(16), 4173–4222. https://doi.org/10.5194/bg-17-4173-2020

Arora, V. K., & Montenegro, A. (2011). Small temperature benefits provided by realistic afforestation efforts. *Nature Geoscience*, *4*(8), 514–518. https://doi.org/10.1038/ngeo1182

Atkin, O. K., Atkinson, L. J., Fisher, R. A., Campbell, C. D., Zaragoza-Castells, J., Pitchford, J. W., et al. (2008). Using temperature-dependent changes in leaf scaling relationships to quantitatively account for thermal acclimation of respiration in a coupled global climate–vegetation model. *Global Change Biology*, *14*(11), 2709–2726. https://doi.org/10.1111/j.1365-2486.2008.01664.x

Atkin, O. K., Bloomfield, K. J., Reich, P. B., Tjoelker, M. G., Asner, G. P., Bonal, D., et al. (2015). Global variability in leaf respiration in relation to climate, plant functional types and leaf traits. *New Phytologist*, *206*(2), 614–636. https://doi.org/10.1111/nph.13253

Atkin, O. K., Evans, J. R., & Siebke, K. (1998). Relationship between the inhibition of leaf respiration by light and enhancement of leaf dark respiration following light treatment. *Australian Journal of Plant Physiology*, *25*(4), 437–443. https://doi.org/10.1071/pp97159

Atkin, O. K., Meir, P., & Turnbull, M. H. (2014). Improving representation of leaf respiration in large-scale predictive climate-vegetation models. *New Phytologist*, *202*(3), 743–748. https://doi.org/10.1111/nph.12686

Atkin, O. K., & Tjoelker, M. G. (2003). Thermal acclimation and the dynamic response of plant respiration to temperature. *Trends in Plant Science*, *8*(7), 343–351. https://doi.org/10.1016/S1360-1385(03)00136-5

Bagley, J., Rosenthal, D. M., Ruiz-Vera, U. M., Siebers, M. H., Kumar, P., Ort, D. R., & Bernacchi, C. J. (2015). The influence of photosynthetic acclimation to rising CO_2 and warmer temperatures on leaf and canopy photosynthesis models. *Global Biogeochemical Cycles*, *29*(2), 194–206. https://doi.org/10.1002/2014GB004848

Bahar, N. H. A., Ishida, F. Y., Weerasinghe, L. K., Guerrieri, R., O'Sullivan, O. S., Bloomfield, K. J., et al. (2017). Leaf-level photosynthetic capacity in lowland Amazonian and high-elevation Andean tropical moist forests of Peru. *New Phytologist*, *214*(3), 1002–1018. https://doi.org/10.1111/nph.14079

Ball, J. T., Woodrow, I. E., & Berry, J. A. (1987). A model predicting stomatal conductance and its contribution to the control of photosynthesis under different environmental conditions. In J. Biggins (Ed.), *Progress in photosynthesis research* (Vol. 4, pp. 221–224). Springer Netherlands. https://doi.org/10.1007/978-94-017-0519-6_48

Beaudoing, H., & Rodell, M. (2020). GLDAS Noah land surface model L4 monthly 0.25 x 0.25 degree V2.1 [Dataset]. *Goddard Earth Sciences Data and Information Services Center (GES DISC)*. https://doi.org/10.5067/SXAVCZFAQLNO

Beer, C., Reichstein, M., Tomelleri, E., Ciais, P., Jung, M., Carvalhais, N., et al. (2010). Terrestrial gross carbon dioxide uptake: Global distribution and covariation with climate. *Science*, *329*(5993), 834–838. https://doi.org/10.1126/science.1184984

Bernacchi, C. J., Pimentel, C., & Long, S. P. (2003). In vivo temperature response functions of parameters required to model RuBP-limited photosynthesis. *Plant, Cell and Environment*, *26*(9), 1419–1430. https://doi.org/10.1046/j.0016-8025.2003.01050.x

Bonan, G. B. (2008). Forests and climate change: Forcings, feedbacks, and the climate benefits of forests. *Science*, *320*(5882), 1444–1449. https://doi.org/10.1126/science.1155121

Bonan, G. B., & Doney, S. C. (2018). Climate, ecosystems, and planetary futures: The challenge to predict life in Earth system models. *Science*, *359*(6375), eaam8328. https://doi.org/10.1126/science.aam8328

Bonan, G. B., & Levis, S. (2010). Quantifying carbon-nitrogen feedbacks in the community land model (CLM4). *Geophysical Research Letters*, *37*(7), L07401. https://doi.org/10.1029/2010GL042430

Bonan, G. B., Levis, S., Sitch, S., Vertenstein, M., & Oleson, K. W. (2003). A dynamic global vegetation model for use with climate models: Concepts and description of simulated vegetation dynamics. *Global Change Biology*, *9*(11), 1543–1566. https://doi.org/10.1046/j.1365-2486.2003.00681.x

Butler, E. E., Wythers, K. R., Flores-Moreno, H., Chen, M., Datta, A., Ricciuto, D. M., et al. (2021). Updated respiration routines alter spatio-temporal patterns of carbon cycling in a global land surface model. *Environmental Research Letters*, *16*(10), 104015. https://doi.org/10.1088/1748-9326/ac2528

Cai, W., & Prentice, I. C. (2020). Recent trends in gross primary production and their drivers: Analysis and modelling at flux-site and global scales. *Environmental Research Letters*, *15*(12), 124050. https://doi.org/10.1088/1748-9326/abc64e

Campbell, J. E., Berry, J. A., Seibt, U., Smith, S. J., Montzka, S. A., Launois, T., et al. (2017). Large historical growth in global terrestrial gross primary production. *Nature*, *544*(7648), 84–87. https://doi.org/10.1038/nature22030

Canadell, J. G., Monteiro, P. M. S., Costa, M. H., Cotrim da Cunha, L., Cox, P. M., Eliseev, A. V., et al. (2021). Global carbon and other biogeochemical cycles and feedbacks. In V. Masson-Delmotte, P. Zhai, A. Pirani, S. L. Connors, C. Péan, S. Berger, et al. (Eds.), *Climate change 2021: The physical science basis. Contribution of working group I to the Sixth assessment report of the intergovernmental panel on climate change* (pp. 673–816). Cambridge University Press. https://doi.org/10.1017/9781009157896.007

Chen, J.-L., Reynolds, J. F., Harley, P. C., & Tenhunen, J. D. (1993). Coordination theory of leaf nitrogen distribution in a canopy. *Oecologia*, *93*(1), 63–69. https://doi.org/10.1007/BF00321192

Chen, W., Wang, S., Wang, J., Xia, J., Luo, Y., Yu, G., & Niu, S. (2023). Evidence for widespread thermal optimality of ecosystem respiration. *Nature Ecology & Evolution*, *7*(9), 1379–1387. https://doi.org/10.1038/s41559-023-02121-w

Ciais, P., Reichstein, M., Viovy, N., Granier, A., Ogée, J., Allard, V., et al. (2005). Europe-wide reduction in primary productivity caused by the heat and drought in 2003. *Nature*, *437*(7058), 529–533. https://doi.org/10.1038/nature03972

Clark, D. B., Mercado, L. M., Sitch, S., Jones, C. D., Gedney, N., Best, M. J., et al. (2011). The Joint UK Land Environment Simulator (JULES), model description – Part 2: Carbon fluxes and vegetation dynamics. *Geoscientific Model Development*, *4*(3), 701–722. https://doi.org/10.5194/gmd-4-701-2011

Collalti, A., Ibrom, A., Stockmarr, A., Cescatti, A., Alkama, R., Fernández-Martínez, M., et al. (2020). Forest production efficiency increases with growth temperature. *Nature Communications*, *11*(1), 5322. https://doi.org/10.1038/s41467-020-19187-w

Collatz, G. J., Ball, J. T., Grivet, C., & Berry, J. A. (1991). Physiological and environmental regulation of stomatal conductance, photosynthesis and transpiration: A model that includes a laminar boundary layer. *Agricultural and Forest Meteorology*, *54*(2), 107–136. https://doi.org/10.1016/0168-1923(91)90002-8

Collatz, G. J., Berry, J. A., & Clark, J. S. (1998). Effects of climate and atmospheric CO_2 partial pressure on the global distribution of C_4 grasses: Present, past, and future. *Oecologia*, *114*(4), 441–454. https://doi.org/10.1007/s004420050468

Crous, K. Y., Drake, J. E., Aspinwall, M. J., Sharwood, R. E., Tjoelker, M. G., & Ghannoum, O. (2018). Photosynthetic capacity and leaf nitrogen decline along a controlled climate gradient in provenances of two widely distributed *Eucalyptus* species. *Global Change Biology*, *24*(10), 4626–4644. https://doi.org/10.1111/gcb.14330

Crous, K. Y., Uddling, J., & De Kauwe, M. G. (2022). Temperature responses of photosynthesis and respiration in evergreen trees from boreal to tropical latitudes. *New Phytologist*, *234*(2), 353–374. https://doi.org/10.1111/nph.17951

Cucchi, M., Weedon, G. P., Amici, A., Bellouin, N., Lange, S., Müller Schmied, H., et al. (2022). Near surface meteorological variables from 1979 to 2019 derived from bias-corrected reanalysis (Version 2.1) [Dataset]. *Copernicus Climate Change Service (C3S) Climate Data Store (CDS)*. https://doi.org/10.24381/cds.20d54e34

Das, R., Chaturvedi, R. K., Roy, A., Karmakar, S., & Ghosh, S. (2023). Warming inhibits increases in vegetation net primary productivity despite greening in India. *Scientific Reports*, *13*(1), 21309. https://doi.org/10.1038/s41598-023-48614-3

Dong, N., Wright, I. J., Chen, J. M., Luo, X., Wang, H., Keenan, T. F., et al. (2022). Rising CO_2 and warming reduce global canopy demand for nitrogen. *New Phytologist*, *235*(5), 1692–1700. https://doi.org/10.1111/nph.18076

Doughty, C. E., & Goulden, M. L. (2008). Seasonal patterns of tropical forest leaf area index and CO_2 exchange. *Journal of Geophysical Research*, *113*(G1), G00B06. https://doi.org/10.1029/2007JG000590

Farquhar, G. D., von Caemmerer, S., & Berry, J. A. (1980). A biochemical model of photosynthetic CO_2 assimilation in leaves of C_3 species. *Planta*, *149*(1), 78–90. https://doi.org/10.1007/BF00386231

Fisher, R. A., & Koven, C. D. (2020). Perspectives on the future of Land Surface Models and the challenges of representing complex terrestrial systems. *Journal of Advances in Modeling Earth Systems*, *12*(4), e2018MS001453. https://doi.org/10.1029/2018ms001453

Franklin, O., Harrison, S. P., Dewar, R., Farrior, C. E., Brännström, Å., Dieckmann, U., et al. (2020). Organizing principles for vegetation dynamics. *Nature Plants*, *6*(5), 444–453. https://doi.org/10.1038/s41477-020-0655-x

Friedlingstein, P., Cox, P., Betts, R., Bopp, L., von Bloh, W., Brovkin, V., et al. (2006). Climate carbon cycle feedback analysis: Results from the C4MIP Model Intercomparison. *Journal of Climate*, *19*(14), 3337–3353. https://doi.org/10.1175/JCLI3800.1

Fung, I. Y., Doney, S. C., Lindsay, K., & John, J. (2005). Evolution of carbon sinks in a changing climate. *Proceedings of the National Academy of Sciences*, *102*(32), 11201–11206. https://doi.org/10.1073/pnas.0504949102

Gao, S., Zhong, R., Yan, K., Ma, X., Chen, X., Pu, J., et al. (2023). Evaluating the saturation effect of vegetation indices in forests using 3D radiative transfer simulations and satellite observations. *Remote Sensing of Environment*, *295*, 113665. https://doi.org/10.1016/j.rse.2023.113665

Ghannoum, O., von Caemmerer, S., Barlow, E. W. R., & Conroy, J. P. (1997). The effect of CO_2 enrichment and irradiance on the growth, morphology and gas exchange of a C3 (Panicum laxum) and a C4 (Panicum antidotale) grass. *Australian Journal of Plant Physiology*, *24*(2), 227–237. https://doi.org/10.1071/PP96077

Harrison, S. P., Cramer, W., Franklin, O., Prentice, I. C., Wang, H., Brännström, Å., et al. (2021). Eco-evolutionary optimality as a means to improve vegetation and land-surface models. *New Phytologist*, *231*(6), 2125–2141. https://doi.org/10.1111/nph.17558

Haverd, V., Smith, B., Nieradzik, L., Briggs, P. R., Woodgate, W., Trudinger, C. M., et al. (2018). A new version of the CABLE land surface model (Subversion revision r4601) incorporating land use and land cover change, woody vegetation demography, and a novel optimisation-based approach to plant coordination of photosynthesis. *Geoscience Model Development*, *11*(7), 2995–3026. https://doi.org/10.5194/gmd-11-2995-2018

Haxeltine, A., & Prentice, I. C. (1996). A general model for the light-use efficiency of primary production. *Functional Ecology*, *10*(5), 551–561. https://doi.org/10.2307/2390165

He, Y., Piao, S., Li, X., Chen, A., & Qin, D. (2018). Global patterns of vegetation carbon use efficiency and their climate drivers deduced from MODIS satellite data and process-based models. *Agricultural and Forest Meteorology*, *256–257*, 150–158. https://doi.org/10.1016/j.agrformet.2018.03.009

Heskel, M. A., O'Sullivan Odhran, S., Reich Peter, B., Tjoelker Mark, G., Weerasinghe Lasantha, K., Penillard, A., et al. (2016). Convergence in the temperature response of leaf respiration across biomes and plant functional types. *Proceedings of the National Academy of Sciences*, *113*(14), 3832–3837. https://doi.org/10.1073/pnas.1520282113

Huntingford, C., Atkin, O. K., Martinez-de la Torre, A., Mercado, L. M., Heskel, M. A., Harper, A. B., et al. (2017). Implications of improved representations of plant respiration in a changing climate. *Nature Communications*, *8*(1), 1602. https://doi.org/10.1038/s41467-017-01774-z

Huo, X., Fox, A. M., Dashti, H., Devine, C., Gallery, W., Smith, W. K., et al. (2024). Integrating state data assimilation and innovative model parameterization reduces simulated carbon uptake in the Arctic and boreal region. *Journal of Geophysical Research: Biogeosciences*, *129*(9), e2024JG008004. https://doi.org/10.1029/2024JG008004

Jia, K., Liang, S., Liu, S., Li, Y., Xiao, Z., Yao, Y., et al. (2015). Global land surface fractional vegetation cover estimation using general regression neural networks from MODIS surface reflectance. *IEEE Transactions on Geoscience and Remote Sensing*, *53*(9), 4787–4796. https://doi.org/10.1109/TGRS.2015.2409563

Jiang, C., & Ryu, Y. (2016). Multi-scale evaluation of global gross primary productivity and evapotranspiration products derived from Breathing Earth System Simulator (BESS). *Remote Sensing of Environment*, *186*, 528–547. https://doi.org/10.1016/j.rse.2016.08.030

Jiang, C., Ryu, Y., Wang, H., & Keenan, T. F. (2020). An optimality-based model explains seasonal variation in C_3 plant photosynthetic capacity. *Global Change Biology*, *26*(11), 6493–6510. https://doi.org/10.1111/gcb.15276

Kattge, J., & Knorr, W. (2007). Temperature acclimation in a biochemical model of photosynthesis: A reanalysis of data from 36 species. *Plant, Cell and Environment*, *30*(9), 1176–1190. https://doi.org/10.1111/j.1365-3040.2007.01690.x

Keenan, T. F., & Niinemets, Ü. (2016). Global leaf trait estimates biased due to plasticity in the shade. *Nature Plants*, *3*(1), 16201. https://doi.org/10.1038/nplants.2016.201

Keenan, T. F., & Williams, C. A. (2018). The terrestrial carbon sink. *Annual Review of Environment and Resources*, *43*(1), 219–243. https://doi.org/10.1146/annurev-environ-102017-030204

Krinner, G., Viovy, N., de Noblet-Ducoudré, N., Ogée, J., Polcher, J., Friedlingstein, P., et al. (2005). A dynamic global vegetation model for studies of the coupled atmosphere-biosphere system. *Global Biogeochemical Cycles*, *19*(1), GB1015. https://doi.org/10.1029/2003GB002199

Kumarathunge, D. P., Medlyn, B. E., Drake, J. E., Tjoelker, M. G., Aspinwall, M. J., Battaglia, M., et al. (2019). Acclimation and adaptation components of the temperature dependence of plant photosynthesis at the global scale. *New Phytologist*, *222*(2), 768–784. https://doi.org/10.1111/nph.15668

Lamour, J., Davidson, K. J., Ely, K. S., Le Moguédec, G., Anderson, J. A., Li, Q., et al. (2023). The effect of the vertical gradients of photosynthetic parameters on the CO assimilation and transpiration of a Panamanian tropical forest. *New Phytologist*, *238*(6), 2345–2362. https://doi.org/10.1111/nph.18901

Lan, X., Tans, P., & Thoning, K. W. (2024). Trends in globally-averaged CO_2 determined from NOAA global monitoring laboratory measurements [Dataset]. *National Oceanic and Atmospheric Administration*. https://doi.org/10.15138/9N0H-ZH07

Lasslop, G., Reichstein, M., Papale, D., Richardson, A. D., Arneth, A., Barr, A., et al. (2010). Separation of net ecosystem exchange into assimilation and respiration using a light response curve approach: Critical issues and global evaluation. *Global Change Biology*, *16*(1), 187–208. https://doi.org/10.1111/j.1365-2486.2009.02041.x

Lawrence, D. M., Fisher, R. A., Koven, C. D., Oleson, K. W., Swenson, S. C., Bonan, G., et al. (2019). The Community Land Model version 5: Description of new features, benchmarking, and impact of forcing uncertainty. *Journal of Advances in Modeling Earth Systems*, *11*(12), 4245–4287. https://doi.org/10.1029/2018MS001583

Lee, T. D., Reich, P. B., & Bolstad, P. V. (2005). Acclimation of leaf respiration to temperature is rapid and related to specific leaf area, soluble sugars and leaf nitrogen across three temperate deciduous tree species. *Functional Ecology*, *19*(4), 640–647. https://doi.org/10.1111/j.1365-2435.2005.01023.x

Li, S., Lü, S., Gao, Y., & Ao, Y. (2015). The change of climate and terrestrial carbon cycle over Tibetan Plateau in CMIP5 models. *International Journal of Climatology*, *35*(14), 4359–4369. https://doi.org/10.1002/joc.4293

Li, Y., Zhou, L., Wang, S., Chi, Y., & Chen, J. (2018). Leaf temperature and vapour pressure deficit (VPD) driving stomatal conductance and biochemical processes of leaf photosynthetic rate in a subtropical evergreen coniferous plantation. *Sustainability*, *10*(11), 4063. https://doi.org/10.3390/su10114063

Liang, J., Xia, J., Liu, L., & Wan, S. (2013). Global patterns of the responses of leaf-level photosynthesis and respiration in terrestrial plants to experimental warming. *Journal of Plant Ecology*, *6*(6), 437–447.

Liu, B., Wang, X., Liu, Q., Xu, Y., Arslan, A. M., Zheng, D., et al. (2024). Response of leaf day respiration in C4 plants to irradiance and vapour pressure deficit. *Crop and Environment*, *3*(2), 101–111. https://doi.org/10.1016/j.crope.2023.12.001

Lombardozzi, D. L., Bonan, G. B., Smith, N. G., Dukes, J. S., & Fisher, R. A. (2015). Temperature acclimation of photosynthesis and respiration: A key uncertainty in the carbon cycle-climate feedback. *Geophysical Research Letters*, *42*(20), 8624–8631. https://doi.org/10.1002/2015GL065934

Luo, Y., Sherry, R., Zhou, X., & Wan, S. (2009). Terrestrial carbon-cycle feedback to climate warming: Experimental evidence on plant regulation and impacts of biofuel feedstock harvest. *Global Change Biology Bioenergy*, *1*(1), 62–74. https://doi.org/10.1111/j.1757-1707.2008.01005.x

Ma, L., Hurtt, G., Ott, L., Sahajpal, R., Fisk, J., Lamb, R., et al. (2022). Global evaluation of the Ecosystem Demography model (ED v3.0). *Geoscientific Model Development*, *15*(5), 1971–1994. https://doi.org/10.5194/gmd-15-1971-2022

Mack, M. C., Bret-Harte, M. S., Hollingsworth, T. N., Jandt, R. R., Schuur, E. A. G., Shaver, G. R., & Verbyla, D. L. (2011). Carbon loss from an unprecedented Arctic tundra wildfire. *Nature*, *475*(7357), 489–492. https://doi.org/10.1038/nature10283

Maire, V., Martre, P., Kattge, J., Gastal, F., Esser, G., Fontaine, S., & Soussana, J. F. (2012). The coordination of leaf photosynthesis links C and N fluxes in C_3 plant species. *PLoS One*, *7*(6), e38345. https://doi.org/10.1371/journal.pone.0038345

Mäkelä, A., Pulkkinen, M., Kolari, P., Lagergren, F., Berbigier, P., Lindroth, A., et al. (2008). Developing an empirical model of stand GPP with the LUE approach: Analysis of eddy covariance data at five contrasting conifer sites in Europe. *Global Change Biology*, *14*(1), 92–108. https://doi.org/10.1111/j.1365-2486.2007.01463.x

Marečková, M., Barták, M., & Hájek, J. (2019). Temperature effects on photosynthetic performance of Antarctic lichen *Dermatocarpon polyphyllizum*: A chlorophyll fluorescence study. *Polar Biology*, *42*(4), 685–701. https://doi.org/10.1007/s00300-019-02464-w

Meek, D. W., Hatfield, J. L., Howell, T. A., Idso, S. B., & Reginato, R. J. (1984). A generalized relationship between photosynthetically active radiation and solar radiation. *Agronomy Journal*, *76*(6), 939–945. https://doi.org/10.2134/agronj1984.00021962007600060018x

Mekonnen, Z. A., Riley, W. J., Randerson, J. T., Grant, R. F., & Rogers, B. M. (2019). Expansion of high-latitude deciduous forests driven by interactions between climate warming and fire. *Nature Plants*, *5*(9), 952–958. https://doi.org/10.1038/s41477-019-0495-8

Mengoli, G., Agustí-Panareda, A., Boussetta, S., Harrison, S. P., Trotta, C., & Prentice, I. C. (2022). Ecosystem photosynthesis in land-surface models: A first-principles approach incorporating acclimation. *Journal of Advances in Modeling Earth Systems*, *14*(1), e2021MS002767. https://doi.org/10.1029/2021ms002767

Middleby, K. B., Cheesman, A. W., & Cernusak, L. A. (2024). Impacts of elevated temperature and vapour pressure deficit on leaf gas exchange and plant growth across six tropical rainforest tree species. *New Phytologist*, *243*(2), 648–661. https://doi.org/10.1111/nph.19822

Niu, G., Yang, Z., Mitchell, K. E., Chen, F., Ek, M. B., Barlage, M., et al. (2011). The community Noah land surface model with multi-parameterization options (Noah-MP): 1. Model description and evaluation with local-scale measurements. *Journal of Geophysical Research*, *116*(D12), D12109. https://doi.org/10.1029/2010JD015139

Oliver, R. J., Mercado, L. M., Clark, D. B., Huntingford, C., Taylor, C. M., Vidale, P. L., et al. (2022). Improved representation of plant physiology in the JULES-vn5.6 land surface model: Photosynthesis, stomatal conductance and thermal acclimation. *Geoscience Model Development*, *15*(14), 5567–5592. https://doi.org/10.5194/gmd-15-5567-2022

Pastorello, G., Trotta, C., Canfora, E., Chu, H., Christianson, D., Cheah, Y.-W., et al. (2020). The FLUXNET2015 dataset and the ONEFlux processing pipeline for eddy covariance data. *Scientific Data*, *7*(1), 225. https://doi.org/10.1038/s41597-020-0534-3

Peng, F., Jung, C. G., Jiang, L., Xue, X., & Luo, Y. (2019). Thermal acclimation of leaf respiration varies between legume and non-legume herbaceous. *Journal of Plant Ecology*, *12*(3), 498–506. https://doi.org/10.1093/jpe/rty042

Peng, Y., Bloomfield, K. J., Cernusak, L. A., Domingues, T. F., & Colin Prentice, I. (2021). Global climate and nutrient controls of photosynthetic capacity. *Communications Biology*, *4*(1), 462. https://doi.org/10.1038/s42003-021-01985-7

Peng, Y., Bloomfield, K. J., & Prentice, I. C. (2020). A theory of plant function helps to explain leaf-trait and productivity responses to elevation. *New Phytologist*, *226*(5), 1274–1284. https://doi.org/10.1111/nph.16447

Piao, S., Fang, J., Ciais, P., Peylin, P., Huang, Y., Sitch, S., & Wang, T. (2009). The carbon balance of terrestrial ecosystems in China. *Nature*, *458*(7241), 1009–1013. https://doi.org/10.1038/nature07944

Piao, S., Luyssaert, S., Ciais, P., Janssens, I. A., Chen, A., Cao, C., et al. (2010). Forest annual carbon cost: A global-scale analysis of autotrophic respiration. *Ecology*, *91*(3), 652–661. https://doi.org/10.1890/08-2176.1

Prentice, I. C., Dong, N., Gleason, S. M., Maire, V., & Wright, I. J. (2014). Balancing the costs of carbon gain and water transport: Testing a new theoretical framework for plant functional ecology. *Ecology Letters*, *17*(1), 82–91. https://doi.org/10.1111/ele.12211

Qiao, S., Wang, H., Prentice, I. C., & Harrison, S. P. (2020). Extending a first-principles primary production model to predict wheat yields. *Agricultural and Forest Meteorology*, *287*, 107932. https://doi.org/10.1016/j.agrformet.2020.107932

Reich, P. B., Sendall, K. M., Stefanski, A., Wei, X., Rich, R. L., & Montgomery, R. A. (2016). Boreal and temperate trees show strong acclimation of respiration to warming. *Nature*, *531*(7596), 633–636. https://doi.org/10.1038/nature17142

Reich, P. B., Stefanski, A., Rich, R. L., Sendall, K. M., Wei, X., Zhao, C., et al. (2021). Assessing the relevant time frame for temperature acclimation of leaf dark respiration: A test with 10 boreal and temperate species. *Global Change Biology*, *27*(12), 2945–2958. https://doi.org/10.1111/gcb.15609

Reich, P. B., Walters, M. B., Ellsworth, D. S., Vose, J. M., Volin, J. C., Gresham, C., & Bowman, W. D. (1998). Relationships of leaf dark respiration to leaf nitrogen, specific leaf area and leaf life-span: A test across biomes and functional groups. *Oecologia*, *114*(4), 471–482. https://doi.org/10.1007/s004420050471

Ren, Y., Wang, H., Harrison, S. P., Prentice, I. C., Atkin, O. K., Smith, N. G., et al. (2023). Reduced global plant respiration due to the acclimation of leaf dark respiration coupled with photosynthesis. *New Phytologist*, *241*(2), 578–591. https://doi.org/10.1111/nph.19355

Rodell, M., Houser, P. R., Jambor, U., Gottschalck, J., Mitchell, K., Meng, C. J., et al. (2004). The global land data assimilation system. *Bulletin of the American Meteorological Society*, *85*(3), 381–394. https://doi.org/10.1175/BAMS-85-3-381

Rogers, A., Medlyn, B. E., Dukes, J. S., Bonan, G., von Caemmerer, S., Dietze, M. C., et al. (2017). A roadmap for improving the representation of photosynthesis in Earth system models. *New Phytologist*, *213*(1), 22–42. https://doi.org/10.1111/nph.14283

Ruehr, S., Keenan, T. F., Williams, C., Zhou, Y., Lu, X., Bastos, A., et al. (2023). Evidence and attribution of the enhanced land carbon sink. *Nature Reviews Earth & Environment*, *4*(8), 518–534. https://doi.org/10.1038/s43017-023-00456-3

Sage, R. F., Sharkey, T. D., & Seemann, J. R. (1989). Acclimation of photosynthesis to elevated carbon dioxide in five C3 species. *Plant Physiology*, *89*(2), 590–596. https://doi.org/10.1104/pp.89.2.590

Sandoval, D., Flo, V., Morfopoulos, C., & Prentice, I. C. (2023). Temperature effects on the global patterns of photosynthetic quantum efficiency. *bioRxiv*. https://doi.org/10.1101/2023.11.11.566568

Scafaro, A. P., Xiang, S., Long, B. M., Bahar, N. H. A., Weerasinghe, L. K., Creek, D., et al. (2017). Strong thermal acclimation of photosynthesis in tropical and temperate wet-forest tree species: The importance of altered Rubisco content. *Global Change Biology*, *23*(7), 2783–2800. https://doi.org/10.1111/gcb.13566

Schober, P., Boer, C., & Schwarte, L. A. (2018). Correlation coefficients: Appropriate use and interpretation. *Anesthesia & Analgesia*, *126*(5), 1763–1768. https://doi.org/10.1213/ANE.0000000000002864

Scott, H. G., & Smith, N. G. (2022). A model of C_4 photosynthetic acclimation based on least-cost optimality theory suitable for Earth System Model incorporation. *Journal of Advances in Modeling Earth Systems*, *14*(3), e2021MS002470. https://doi.org/10.1029/2021MS002470

Sellers, P. J., Berry, J. A., Collatz, G. J., Field, C. B., & Hall, F. G. (1992). Canopy reflectance, photosynthesis, and transpiration. III. A reanalysis using improved leaf models and a new canopy integration scheme. *Remote Sensing of Environment*, *42*(3), 187–216. https://doi.org/10.1016/0034-4257(92)90102-P

Seyednasrollah, B., Young, A. M., Hufkens, K., Milliman, T., Friedl, M. A., Frolking, S., & Richardson, A. D. (2019). Tracking vegetation phenology across diverse biomes using Version 2.0 of the PhenoCam Dataset. *Scientific Data*, *6*(1), 222. https://doi.org/10.1038/s41597-019-0229-9

Shangguan, W., & Dai, Y. (2014). The global soil dataset for earth system modeling (2014) [Dataset]. *A Big Earth Data Platform for Three Poles*. https://doi.org/10.11888/Soil.tpdc.270578

Sitch, S., Friedlingstein, P., Gruber, N., Jones, S. D., Murray-Tortarolo, G., Ahlström, A., et al. (2015). Recent trends and drivers of regional sources and sinks of carbon dioxide. *Biogeosciences*, *12*(3), 653–679. https://doi.org/10.5194/bg-12-653-2015

Slot, M., & Kitajima, K. (2015). General patterns of acclimation of leaf respiration to elevated temperatures across biomes and plant types. *Oecologia*, *177*(3), 885–900. https://doi.org/10.1007/s00442-014-3159-4

Smith, N. G., & Dukes, J. S. (2017). LCE: Leaf carbon exchange data set for tropical, temperate, and boreal species of North and Central America. *Ecology*, *98*(11), 2978. https://doi.org/10.1002/ecy.1992

Smith, N. G., Keenan, T. F., Colin Prentice, I., Wang, H., Wright, I. J., Niinemets, U., et al. (2019). Global photosynthetic capacity is optimized to the environment. *Ecology Letters*, *22*(3), 506–517. https://doi.org/10.1111/ele.13210

Smith, N. G., Zhu, Q., Keenan, T. F., & Riley, W. J. (2024). Acclimation of photosynthesis to CO_2 increases ecosystem carbon storage due to leaf nitrogen savings. *Global Change Biology*, *30*(11), e17558. https://doi.org/10.1111/gcb.17558

Stitt, M., & Schulze, D. (1994). Does Rubisco control the rate of photosynthesis and plant growth? An exercise in molecular ecophysiology. *Plant, Cell and Environment*, *17*(5), 465–487. https://doi.org/10.1111/j.1365-3040.1994.tb00144.x

Stocker, B. D., Wang, H., Smith, N. G., Harrison, S. P., Keenan, T. F., Sandoval, D., et al. (2020). P-Model v1.0: An optimality-based light use efficiency model for simulating ecosystem gross primary production. *Geoscience Model Development*, *13*(3), 1545–1581. https://doi.org/10.5194/gmd-13-1545-2020

Tissue, D. T., Thomas, R. B., & Strain, B. R. (1993). Long-term effects of elevated CO_2 and nutrients on photosynthesis and Rubisco in loblolly pine seedlings. *Plant, Cell and Environment*, *16*(7), 859–865. https://doi.org/10.1111/j.1365-3040.1993.tb00508.x

Togashi, H. F., Prentice, I. C., Atkin, O. K., Macfarlane, C., Prober, S. M., Bloomfield, K. J., & Evans, B. J. (2018). Thermal acclimation of leaf photosynthetic traits in an evergreen woodland, consistent with the coordination hypothesis. *Biogeosciences*, *15*(11), 3461–3474. https://doi.org/10.5194/bg-15-3461-2018

Turnbull, M. H., Murthy, R., & Griffin, K. L. (2002). The relative impacts of daytime and night-time warming on photosynthetic capacity in Populus deltoides. *Plant, Cell and Environment*, *25*(12), 1729–1737. https://doi.org/10.1046/j.1365-3040.2002.00947.x

VEMAP. (1995). Vegetation/Ecosystem Modeling and Analysis Project: Comparing biogeography and biogeochemistry models in a continental-scale study of terrestrial ecosystem responses to climate change and CO_2 doubling. *Global Biogeochemical Cycles*, *9*(4), 407–437. https://doi.org/10.1029/95GB02746

Virkkala, A.-M., Rogers, B. M., Watts, J. D., Arndt, K. A., Potter, S., Wargowsky, I., et al. (2024). An increasing Arctic-boreal CO_2 sink offset by wildfires and source regions. *bioRxiv*. https://doi.org/10.1101/2024.02.09.579581

von Caemmerer, S., & Farquhar, G. D. (1981). Some relationships between the biochemistry of photosynthesis and the gas exchange of leaves. *Planta*, *153*(4), 376–387. https://doi.org/10.1007/BF00384257

Vuichard, N., Messina, P., Luyssaert, S., Guenet, B., Zaehle, S., Ghattas, J., et al. (2019). Accounting for carbon and nitrogen interactions in the global terrestrial ecosystem model ORCHIDEE (trunk version, rev 4999): Multi-scale evaluation of gross primary production. *Geoscientific Model Development*, *12*(11), 4751–4779. https://doi.org/10.5194/gmd-12-4751-2019

Walker, A. P., Beckerman, A. P., Gu, L., Kattge, J., Cernusak, L. A., Domingues, T. F., et al. (2014). The relationship of leaf photosynthetic traits - Vcmax and Jmax - To leaf nitrogen, leaf phosphorus, and specific leaf area: A meta-analysis and modeling study. *Ecology and Evolution*, *4*(16), 3218–3235. https://doi.org/10.1002/ece3.1173

Wang, H., Atkin, O. K., Keenan, T. F., Smith, N. G., Wright, I. J., Bloomfield, K. J., et al. (2020). Acclimation of leaf respiration consistent with optimal photosynthetic capacity. *Global Change Biology*, *26*(4), 2573–2583. https://doi.org/10.1111/gcb.14980

Wang, H., Prentice, I. C., Keenan, T. F., Davis, T. W., Wright, I. J., Cornwell, W. K., et al. (2017). Towards a universal model for carbon dioxide uptake by plants. *Nature Plants*, *3*(9), 734–741. https://doi.org/10.1038/s41477-017-0006-8

Wang, J. A., Baccini, A., Farina, M., Randerson, J. T., & Friedl, M. A. (2021). Disturbance suppresses the aboveground carbon sink in North American boreal forests. *Nature Climate Change*, *11*(5), 435–441. https://doi.org/10.1038/s41558-021-01027-4

Wang, K., Piao, S., He, Y., Liu, Y., & He, H. (2023). Spatial variations and mechanisms for the stability of terrestrial carbon sink in China. *Science China Earth Sciences*, *66*(2), 227–236. https://doi.org/10.1007/s11430-021-1003-5

Wang, N., Quesada, B., Xia, L., Butterbach-Bahl, K., Goodale, C. L., & Kiese, R. (2019). Effects of climate warming on carbon fluxes in grasslands—A global meta-analysis. *Global Change Biology*, *25*(5), 1839–1851. https://doi.org/10.1111/gcb.14603

Wang, W., Wang, J., Liu, X., Zhou, G., & Yan, J. (2016). Decadal drought deaccelerated the increasing trend of annual net primary production in tropical or subtropical forests in southern China. *Scientific Reports*, *6*(1), 28640. https://doi.org/10.1038/srep28640

Wang, X., Chen, J. M., Ju, W., & Zhang, Y. (2022). Seasonal variations in leaf maximum photosynthetic capacity and its dependence on climate factors across global FLUXNET sites. *Journal of Geophysical Research: Biogeosciences*, *127*(5), e2021JG006709. https://doi.org/10.1029/2021jg006709

Weerasinghe, L. K., Creek, D., Crous, K. Y., Xiang, S., Liddell, M. J., Turnbull, M. H., & Atkin, O. K. (2014). Canopy position affects the relationships between leaf respiration and associated traits in a tropical rainforest in Far North Queensland. *Tree Physiology*, *34*(6), 564–584. https://doi.org/10.1093/treephys/tpu016

Xu, H., Wang, H., Prentice, I. C., Harrison, S. P., Wang, G., & Sun, X. (2021). Predictability of leaf traits with climate and elevation: A case study in Gongga Mountain, China. *Tree Physiology*, *41*(8), 1336–1352. https://doi.org/10.1093/treephys/tpab003

Yamori, W., Suzuki, K., Noguchi, K., Nakai, M., & Terashima, I. (2006). Effects of Rubisco kinetics and Rubisco activation state on the temperature dependence of the photosynthetic rate in spinach leaves from contrasting growth temperatures. *Plant, Cell and Environment*, *29*(8), 1659–1670. https://doi.org/10.1111/j.1365-3040.2006.01550.x

Yang, Z.-L., Niu, G.-Y., Mitchell, K. E., Chen, F., Ek, M. B., Barlage, M., et al. (2011). The community Noah land surface model with multiparameterization options (Noah-MP): 2. Evaluation over global river basins. *Journal of Geophysical Research*, *116*(D12), D12110. https://doi.org/10.1029/2010JD015140

YanghangRen. (2025). YanghangRen/NoahMP-EEO-code: V1.0 (V1.0) [Dataset]. *Zenodo*. https://doi.org/10.5281/zenodo.14674455

Yuan, H., Dai, Y., Xiao, Z., Ji, D., & Shangguan, W. (2011). Reprocessing the MODIS Leaf Area Index products for land surface and climate modelling. *Remote Sensing of Environment*, *115*(5), 1171–1187. https://doi.org/10.1016/j.rse.2011.01.001

Zhang, Z., Ju, W., Li, X., Cheng, X., Zhou, Y., Xu, S., et al. (2024). Joint improvement on absorbed photosynthetically active radiation and intrinsic quantum yield efficiency algorithms in the P model betters the estimate of terrestrial gross primary productivity. *Agricultural and Forest Meteorology*, *346*, 109883. https://doi.org/10.1016/j.agrformet.2023.109883

Zhang-Zheng, H., Deng, X., Aguirre-Gutiérrez, J., Stocker, B. D., Thomson, E., Ding, R., et al. (2024). Why models underestimate West African tropical forest primary productivity. *Nature Communications*, *15*(1), 9574. https://doi.org/10.1038/s41467-024-53949-0

Zhao, L., Gao, X., An, Q., Ren, X., Zhang, Y., Luo, L., et al. (2023). A shift from isohydric to anisohydric water-use strategy as a result of increasing drought stress for young apple trees in a semiarid agroforestry system. *Agricultural and Forest Meteorology*, *336*, 109484. https://doi.org/10.1016/j.agrformet.2023.109484

Zhao, M., & Running, S. W. (2010). Drought-induced reduction in global terrestrial net primary production from 2000 through 2009. *Science*, *329*(5994), 940–943. https://doi.org/10.1126/science.1192666

Zheng, Y., Shen, R., Wang, Y., Li, X., Liu, S., Liang, S., et al. (2020). Improved estimate of global gross primary production for reproducing its long-term variation, 1982-2017. *Earth System Science Data*, *12*(4), 2725–2746. https://doi.org/10.5194/essd-12-2725-2020

Zhu, L., Bloomfield, K. J., Asao, S., Tjoelker, M. G., Egerton, J. J. G., Hayes, L., et al. (2021). Acclimation of leaf respiration temperature responses across thermally contrasting biomes. *New Phytologist*, *229*(3), 1312–1325. https://doi.org/10.1111/nph.16929

Zhu, Q., Riley, W. J., Tang, J., Collier, N., Hoffman, F. M., Yang, X., & Bisht, G. (2019). Representing nitrogen, phosphorus, and carbon interactions in the E3SM land model: Development and global benchmarking. *Journal of Advances in Modeling Earth Systems*, *11*(7), 2238–2258. https://doi.org/10.1029/2018MS001571

Zhu, Z., Wang, H., Harrison, S. P., Prentice, I. C., Qiao, S., & Tan, S. (2023). Optimality principles explaining divergent responses of alpine vegetation to environmental change. *Global Change Biology*, *29*(1), 126–142. https://doi.org/10.1111/gcb.16459

References From the Supporting Information

Bernacchi, C. J., Singsaas, E. L., Pimentel, C., Portis, A. R., Jr., & Long, S. P. (2001). Improved temperature response functions for models of Rubisco-limited photosynthesis. *Plant, Cell and Environment*, *24*(2), 253–259. https://doi.org/10.1111/j.1365-3040.2001.00668.x

Huber, M. L., Perkins, R. A., Laesecke, A., Friend, D. G., Sengers, J. V., Assael, M. J., et al. (2009). New international formulation for the viscosity of H_2O. *Journal of Physical and Chemical Reference Data*, *38*(2), 101–125. https://doi.org/10.1063/1.3088050

Jordan, R. E. (1991). A one-dimensional temperature model for a snow cover: Technical documentation for SNTHERM.89. *Cold Region Research and Engineering Laboratory, U.S. Army Corps of Engineers*.

Sakaguchi, K., & Zeng, X. (2009). Effects of soil wetness, plant litter, and under-canopy atmospheric stability on ground evaporation in the Community Land Model (CLM3.5). *Journal of Geophysical Research*, *114*(D1), D01107. https://doi.org/10.1029/2008JD010834